Lindemann criterion and vortex lattice phase transitions in type-II superconductors

Jan Kierfeld

Max-Planck-Institut für Kolloid- und Grenzflächenforschung, 14424 Potsdam, Germany

Valerii Vinokur

Argonne National Laboratory, Materials Science Division, 9700 South Cass Avenue, Argonne, Illinois 60439, USA

We discuss the destruction of vortex lattice order in type-II superconductors by random point pinning and thermal fluctuations based on Lindemann criteria. The location of the melting line and the order-disorder transition, which marks the destruction of the topologically ordered Bragg glass phase and is the reason for the second peak effect, is calculated. We focus on a comparative discussion of different versions of Lindemann criteria and, with regard to experiment, on a comparative discussion of three classes of type-II superconductors—low-T_c, anisotropic high-T_c, and layered high-T_c materials. Specific attention is paid to the role of nonlocal magnetic interlayer couplings and the softening of elastic moduli at high magnetic fields, which is crucial for low-T_c materials. We also discuss in detail the competing mechanisms of thermal depinning and temperature dependence of the pinning strength through microscopic parameters as well as the crossover between single vortex and bundle pinning for low-T_c materials.

I. INTRODUCTION

Influence of quenched random pinning on the crystalline order of the vortex lattice in type-II superconductors is an issue of longstanding interest for theory and experiment because structural properties of the vortex lattice immediately influence quantities crucial for applications, e.g., critical currents and electrical resistance. The flux line array in high-T_c superconductors (HTSC's) such as $Bi_2Sr_2CaCu_2O_{8+x}$ (BSCCO) or $YBa_2Cu_3O_{7-x}$ (YBCO) is extremely susceptible to thermal and disorder-induced fluctuations due to the interplay of several parameters such as high transition temperature T_c, large magnetic penetration depth λ and short coherence length ξ, and a strong anisotropy of the material. This leads to the existence of a variety of fluctuation dominated phases of the flux-line array and very rich phase diagrams for the HTSC materials.[1–3] But also in low-T_c materials such as 2H-NbSe$_2$ (NbSe) structural instabilities of the vortex lattice produce analogous effects in the critical current, however, in much closer vicinity to the upper critical field H_{c2} as compared to high-T_c materials.

Upon increasing the temperature across the melting transition of the vortex lattice the critical current goes to zero and superconductivity is destroyed by thermal fluctuations of the vortex lines. The existence of a melting transition of the flux-line lattice (FLL) into an entangled vortex liquid (VL) was first proposed by Nelson.[4] Observations of hysteretic resistivity switching and magnetization measurements[5] have experimentally supported a first-order melting of very clean lattices. Calculations for the locus of the melting line have been mainly based on the use of the Lindemann criterion $\langle u^2 \rangle_T = c_L^2 a^2$, which estimates the root-mean-square thermal displacement fluctuations $(\langle u^2 \rangle_T)^{1/2}$ of a vortex element at the melting transition as a fraction $c_L a$ of the FLL spacing a with a Lindemann number $c_L \approx 0.2$. The phenomenological Lindemann criterion has proven very successful in describing experimental melting curves, and refined theoretical

evaluations of $\langle u^2 \rangle_T$ have been presented for anisotropic[6] and strongly layered[7] HTSC materials. Recently two melting theories going beyond a Lindemann analysis have been proposed offering two complementary mechanisms for the vortex lattice melting. In Ref. 8 a self-consistent analysis of anharmonicities beyond the elastic deformation of the FLL leads to a melting instability, in Ref. 9 a theory of dislocation-mediated vortex lattice melting is put forward.

Since the work of Larkin and Ovchinnikov,[10] the influence of quenched pointlike pinning centers on the vortex lattice and the nature of the collectively pinned FLL have been subject of intense theoretical interest. It was argued in Refs. 11 and 12 that weak point disorder drives the vortex lattice into a vortex glass (VG) state with zero linear resistivity, which has been supported by experimental findings.[13] In weak collective pinning theory according to Ref. 10, disorder-induced relative displacements grow as $\overline{\langle [u(\mathbf{r}) - u(0)]\rangle^2} \sim r^{4-d}$ in d-dimensional space, i.e., the pinned FLL is described by the roughness exponent $\zeta = (4-d)/2$. This would lead to an instability with respect to the proliferation of topological defects such as dislocations in the FLL (Ref. 14) such that weak point disorder was believed to destroy the crystal order of the FLL. However, the argument does not take into account that the results of Ref. 10 get modified for displacements exceeding the coherence length ξ. On larger length scales the growth of relative displacements first crosses over to a power law with a somewhat smaller ζ,[12] before a very slow *logarithmic* growth sets in on the largest scales.[15,16] In the absence of dislocations this leads to a VG phase that maintains quasi-long-range translational order with power-law Bragg singularities in the structure factor and has thus been called "Bragg glass" (BrG).[16] In Refs. 16–18 it has been argued that the elastic BrG is stable against dislocation formation at low magnetic fields.

Upon increasing the magnetic field the vortex lattice softens and the point disorder strength effectively increases. At sufficiently high magnetic fields the BrG becomes unstable

and dislocations proliferate.[9,17,18] Various experimental signatures can be attributed to the resulting order-disorder or amorphization transition into a high-field *amorphous* VG. Neutron-diffraction measurements on BSCCO (Ref. 19) show a destruction of the characteristic power-law Bragg peaks at higher fields. Also transport measurements on YBCO (Ref. 20) indicate a crossover from the first-order melting at low magnetic fields to a continuous VG-VL transition that can be related to the order-disorder transition within the vortex solid. The occurrence of a very sharp second peak in magnetic hysteresis measurements on BSCCO,[21] YBCO,[22] or NbSe (Ref. 23) at a well-defined second peak field can be interpreted as another hallmark of the order-disorder transition from a low-field elastic BrG to the high-field amorphous VG. The second peak is associated with a rise of the critical current across this transition which is due to an onset of plastic deformation. It has been shown in Ref. 24 that plastic degrees of freedom depin at lower current densities j but below the depinning threshold barriers $U(j)$ $\sim j^{-\mu}$ are higher, i.e., μ is larger for plastic creep, which can explain the rise in the apparent critical current that manifests in the second peak. This corresponds to the intuitive picture that the additional plastic deformation allows better adjustment of the pinned FLL configuration thus leading to larger critical currents.

Analogously to the case of thermal melting, progress in predicting the locus of the order-disorder or amorphization transition has mainly been made by using generalized phenomenological Lindemann criteria.[25-32] Derivations of Lindemann criteria have been given in Refs. 17 and 9 by studying the onset of the instability of the BrG with respect to spontaneous generation of disorder-induced dislocations. Whereas Refs. 25–30 and 32 focus on high-T_c materials such as BSCCO or YBCO, Ref. 31 addresses also low-T_c materials such as NbSe. In this paper we want to critically review the Lindemann analysis for the three representative materials BSCCO, YBCO, and NbSe with BSCCO as a typical strongly layered high-T_c compound with weak Josephson coupling, YBCO as a typical moderately anisotropic high-T_c, and NbSe as a typical weakly anisotropic low-T_c type-II superconductor. On the one hand, we want to emphasize the common approach via the Lindemann analysis; on the other hand, the comparative study will show that each of the three mentioned classes of superconductors exhibit peculiarities that have to be taken into account in the analysis. At low magnetic fields, when the vortex spacing a becomes larger than the magnetic penetration depth λ, we have to pay specific attention to the role of nonlocal electromagnetic couplings. This becomes particularly important for BSCCO with its weak Josephson coupling where the order-disorder transition takes place at such low fields. In low-T_c materials, on the other hand, the softening of elastic moduli at high magnetic fields is particularly relevant because both melting line and the order-disorder transition are located close to the upper critical field H_{c2}. An important point in interpreting experiments is also a detailed knowledge of the temperature dependence of the order-disorder transition line, which is determined by an interplay between the temperature dependence of microscopic parameters entering the pinning

strength and the effective weakening of the pinning potential by ''thermal smearing'' due to thermal motion of the vortices which can give rise to thermal depinning.[1] Often one or the other source of temperature dependence can be neglected. For example, in low-T_c materials depinning temperatures are very close to T_c and the temperature dependence through microscopic parameters is more important whereas in high-T_c materials thermal depinning is the dominating effect.

The paper is organized as follows. First we will discuss the Lindemann criteria for thermal and disorder-induced melting transitions in Sec. II. In a system subject to quenched disorder the Lindemann criterion can be formulated in two slightly different versions both of which can be interpreted in terms of the underlying melting mechanism: Thermal and quenched fluctuations can act *independently* from each other in destroying the lattice order or they can act *cooperatively*. In Sec. III we will show how the Lindemann criterion for melting of the vortex lattice can be reformulated in terms of fluctuations of *single* vortices of a certain length, the *single-vortex length* L_0, that is set by the interactions within the FLL. In Sec. IV we discuss how the properties of single-vortex fluctuations are strongly modified if the nonlocal electromagnetic coupling cannot be neglected. This becomes crucial in the Lindemann analysis for the strongly high-T_c layered materials, e.g., BSCCO. In Sec. V we present the Lindemann analysis for thermal melting in the absence of quenched disorder, first for YBCO and NbSe, and then for BSCCO. In order to study the order-disorder or amorphization transition that is caused by quenched point disorder employing the single-vortex Lindemann criterion we have to discuss the pinning of single vortices which is done in Sec. VI. Within weak collective pinning theory discussed in Sec. VI A, the characteristic length scale set by the frozen-in point disorder is the *collective pinning* or *Larkin length* L_c. We have to carefully distinguish several pinning regimes depending on the size of the pinning length L_c in comparison to the single-vortex length L_0 and the layer spacing d in a layered material. For $L_c > L_0$ we have *bundle pinning* for $L_c > L_0$ and *single-vortex pinning* for $L_c < L_0$ which are discussed in Sec. VI B. For $L_c < d$ the layered structure becomes relevant for the pinning, and there is a crossover from weak collective pinning to *strong pinning* of pancake vortices which is discussed separately in Sec. VI C. The Lindemann analysis is complicated by the fact that the pinning strength is temperature dependent through two different mechanisms. We have a temperature dependence of the pinning strength through the microscopic parameters (such as λ or ξ) but we also have smearing or weakening of disorder by thermal fluctuations above the *depinning temperature* T_{dp}. Therefore we have to carefully discuss the temperature dependence of the crossover between the different pinning regimes for the three exemplary materials throughout Sec. VI. Having clarified the different pinning regimes we can perform the Lindemann analysis for the order-disorder or amorphization transition driven by the quenched point disorder. This task is split into two parts. In Sec. VII we discuss the analysis for $T=0$ depending on magnetic fields and pinning strength. Finally, in Sec. VIII, we discuss the influence of thermal fluctuations and perform the Lindemann analysis for

$T>0$, i.e., in the familiar B-T plane. In the Appendix we provide a set of values for material parameters used for estimates throughout the text for all three exemplary materials and a list of symbols (Table I).

II. LINDEMANN CRITERION

The phenomenological Lindemann criterion has proven successful[6,7] in determining the locus of the melting transition for the first-order thermal melting transition. At sufficiently low disorder strength or low magnetic fields the first-order thermal melting transition can also be found in the presence of point disorder. In its conventional form for thermal fluctuations the Lindemann criterion is formulated as

$$\langle u^2 \rangle_T = c_L^2 a^2, \qquad (1)$$

where $\mathbf{u}$ is the displacement of vortex elements and $\langle \cdots \rangle_T$ the purely thermal average in the *absence* of quenched disorder. The Lindemann number c_L is introduced here as a phenomenological parameter that is supposed to depend only weakly on the specific lattice parameters of the solid phase, in particular it is assumed to be independent of the magnetic field. In principle its value can be determined by *ab initio* melting theories going beyond a Lindemann analysis, for example, in Ref. 9 a value $c_L \approx 0.2$ is found for dislocation-mediated vortex lattice melting. The Lindemann number c_L can also be determined from simulations of the vortex lattice melting transition. Early Monte Carlo studies of an interacting line model[33] find a melting transition with a Lindemann number that depends weakly on the magnetic field with values $c_L \approx 0.2$ over a wide field range. Path integral Monte Carlo simulations of the corresponding lattice to superfluid transition of two-dimensional (2D) bosons[34] give a Lindemann number $c_L \approx 0.25$. Finally, carefully equilibrated Monte Carlo simulations of the three-dimensional uniformly frustrated, anisotropic XY model[35] give a value of $c_L \approx 0.18$. All these findings suggest that a Lindemann number $c_L \approx 0.2$ is appropriate for the thermal vortex lattice melting. For the disorder-induced transition we will assume similar values of the Lindemann number.

For thermal fluctuations the main contribution to the mean-square displacement comes from fluctuations with the shortest wavelength of the order of the vortex spacing a. Therefore one can rewrite the Lindemann criterion for thermal melting (1) as

$$\langle \Delta u^2(a,0) \rangle_T = \langle [u(\mathbf{a},0) - u(\mathbf{0},0)]^2 \rangle_T = c_L^2 a^2, \qquad (2)$$

where $\mathbf{u}(\mathbf{R},z)$ is the displacement of the vortex element at $\mathbf{r} = (\mathbf{R},z)$, and $\mathbf{a}$ is a unit vector of the hexagonal Abrikosov lattice. z is the coordinate parallel to the magnetic field $\mathbf{H}$ which is directed along the c axis of the anisotropic type-II superconductor in the usual experimental situation, $\mathbf{H} \| \mathbf{c}$. In the form (2), the Lindemann criterion is a *local* criterion where thermal fluctuations in the bond length $a + \Delta u(a,0)$ connecting nearest neighbors are used to indicate the loss of *global* positional order of the FLL. In the form (2) the Lindemann criterion can also be applied to situations where $\langle u^2 \rangle_T$ is formally diverging as, for example, in the thermal
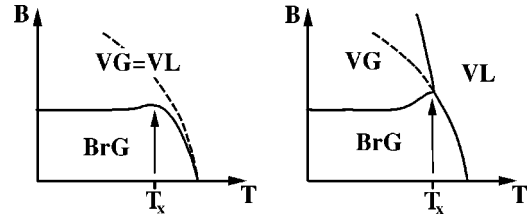

FIG. 1. Schematic phase diagram (neglecting reentrance at low fields) illustrating the two scenarios corresponding to the two possible generalizations of the Lindemann criterion. Left: According to Eq. (3) if temperature and point disorder act cooperatively. Right: According to Eqs. (2), (4), and (5) if temperature and point disorder cause distinct phase transitions. The dashed line is the thermal melting line in the absence of quenched disorder according to Eq. (2). The temperature T_x is defined by $\langle \Delta u^2(a,0) \rangle_T = \overline{\langle \Delta u(a,0) \rangle^2} = c_L^2 a^2$.

melting of a two-dimensional lattice and to the order-disorder transition due to quenched point disorder that we will discuss now.

There are two possibilities to generalize criterion (2) in order to include phenomenologically the disorder-induced quenched displacement fluctuations as possible cause for the destruction of the vortex crystal. To see this we first note that at finite temperatures and in the presence of quenched point disorder the displacement has two parts $\mathbf{u} = \mathbf{u}_p + \mathbf{u}_{th}$ in the notation of Ref. 1. The quenched part $\mathbf{u}_p$ is due to pinning and does not average to zero upon performing the thermal average: $\mathbf{u}_p = \langle \mathbf{u} \rangle$. The part $\mathbf{u}_{th} = \mathbf{u} - \langle \mathbf{u} \rangle$ describes thermal fluctuations around the pinning part. Thus $\overline{\langle u_{th}^2 \rangle} = \overline{\langle u^2 \rangle} - \overline{\langle u \rangle^2}$ is the thermal part and $\overline{u_p^2} = \overline{\langle u \rangle^2}$ the disorder part of the mean-square fluctuations. By using a tilt symmetry of the vortex system[36] one can establish that $\overline{\langle u_{th}^2 \rangle}$ is unchanged by the quenched disorder, i.e., $\overline{\langle u_{th}^2 \rangle} = \langle u^2 \rangle_T$. However, u_{th} is *not* Gaussian distributed as in the absence of quenched disorder.[37]

The first possibility to generalize criterion (2) is to replace $\langle \Delta u^2(a,0) \rangle_T = \overline{\langle \Delta u_{th}^2(a,0) \rangle}$ by the *full* mean-square displacement $\overline{\langle \Delta u^2(a,0) \rangle} = \langle \Delta u_{th}^2(a,0) \rangle + \langle \Delta u_p^2(a,0) \rangle$ in Eq. (1):

$$\overline{\langle \Delta u^2(a,0) \rangle} = \langle \Delta u^2(a,0) \rangle_T + \overline{\langle \Delta u(a,0) \rangle^2} = c_L^2 a^2. \qquad (3)$$

This procedure is suitable if temperature (or entropy) and quenched disorder act *cooperatively* in generating topological defects in the FLL. It corresponds to a scenario where there is only *one* topologically disordered phase beyond the BrG instability, and the VL phase and the amorphous VG are thermodynamically identical phases. A criterion such as Eq. (3) would shift the thermal melting line to lower fields and lead to a *crossover* of the thermal melting line into the amorphization transition line as soon as $\langle \Delta u^2(a,0) \rangle_T = \overline{\langle \Delta u(a,0) \rangle^2} = c_L^2 a^2$ at a temperature T_x, see Fig. 1. A Lindemann criterion of the form (3) has been assumed in almost all previous Lindemann analysis of the BrG stability.[25–28,30–32] It can also be formulated in terms of three characteristic energies of a vortex lattice unit cell,[29,32] the temperature T, a characteristic energy $E_{pl} \propto c_L^2$ necessary for

plastic deformation of the FLL, and a characteristic pinning energy E_{pin} (equations for E_{pl} and E_{pin} will be given below) as $T+E_{pin}=E_{pl}$.

A different possibility to generalize criterion (2) is based on a mechanism where temperature and quenched disorder do not act cooperatively but lead to two *distinct* instabilities of the BrG, for example instabilities with respect to dislocation loops on two different length scales. Such a mechanism has been advocated in Ref. 9 where temperature leads to an instability with respect to a dislocation array of high dislocation density $\rho \sim a^{-3}$, which can be interpreted as a VL phase saturated with small dislocation loops. On the other hand, quenched disorder leads to an instability with respect to a much smaller dislocation density that is essentially set by a large pinning length (the positional correlation length, see Ref. 9) and characterizing the amorphous VG. Having such a scenario in mind one would rather generalize Eq. (1) by introducing a second criterion which considers only the pinning-induced displacements

$$\overline{\langle \Delta u(a,0) \rangle^2} = c_L^2 a^2, \qquad (4)$$

giving the locus of the disorder-induced or amorphization transition line. The locus of the thermal melting line is still given by Eq. (1) or (2) and unchanged by quenched disorder.

Within the scenario where quenched disorder and thermal fluctuations act independently, one consequently argues for *two* distinct topologically disordered phases, the VL and the amorphous VG (at least close to the stability region of the quasiordered BrG, where we expect Lindemann criteria to work, at higher fields a critical end point can occur[9]). This suggests that the locus of the VG-VL transition is given by a third Lindemann-like criterion

$$\langle \Delta u^2(a,0) \rangle_T = \overline{\langle \Delta u(a,0) \rangle^2}, \qquad (5)$$

and we have three-phase coexistence for $\langle \Delta u^2(a,0) \rangle_T = \overline{\langle \Delta u(a,0) \rangle^2} = c_L^2 a^2$ at the temperature T_x, see Fig. 1. Only in the Lindemann analysis of Ref. 29 this second generalization of the Lindemann criterion has been employed consistently although in Ref. 25 a criterion equivalent to Eq. (5) is applied to calculate the irreversibility line [but the BrG phase boundary is calculated using Eq. (3) in Ref. 25]. In Ref. 29 the two Lindemann criteria were formulated in terms of the three characteristic energies that we introduced above. We can write $T=E_{pl}$ equivalent to Eq. (1) as criterion for thermal melting, the BrG-VL transition. $E_{pin}=E_{pl}$ corresponding to Eq. (4) is the criterion for the order-disorder transition line between VL and amorphous VG. Finally $T=E_{pin}$ equivalent to Eq. (5) is the criterion for the VG-VL transition.

Within a dislocation-mediated melting theory it is indeed possible to give some qualitative arguments supporting the view that quenched disorder and thermal fluctuations act *independently* rather than cooperatively in destroying the lattice order. For dislocation-mediated melting it is expected that a first-order transition into a VL phase without any short-scale translational order has to correspond to a phase transition where a dense array of dislocations ($\rho \sim a^{-3}$) enters the sample. On the other hand, in the presence of

quenched disorder dislocation lines gain disorder energy by optimizing their position and shape. However, in a dense dislocation array with dislocation distances or dislocation loop sizes of the order of the lattice spacing a also the optimization of position and shape can only take place over distances of the order of a, and thus give only small additional disorder energy gains compared to the entropic terms. This suggests that quenched disorder is an irrelevant perturbation and that thermal fluctuations $\overline{\langle u_{th}^2 \rangle}$ alone should be considered in the Lindemann criterion, as in Eq. (1). On the other hand, for the melting induced by quenched disorder, thermal fluctuations are irrelevant because in the three-dimensional FLL $\langle u_{th}^2 \rangle$ is independent of system size and thus not diverging in the thermodynamic limit. Therefore we expect temperature to be an irrelevant perturbation at this order-disorder or amorphization transition that causes only thermal smearing of the disorder but does not change the nature of the transition.[1] This suggests that as in Eq. (4) disorder-induced fluctuations $\overline{\langle u \rangle^2}$ alone should be considered in the Lindemann criterion. Note that effects of thermal smearing are taken into account already in expressions such as $\overline{\langle u \rangle^2}$ due to the thermal preaveraging.

The situation is more subtle for related models of elastic manifolds in *two* dimensions.[38,39] There it has been demonstrated rigorously that below a depinning temperature thermal fluctuations are irrelevant and the transition driven by quenched disorder is in the same universality class as the corresponding $T=0$ transition. As in three dimensions temperature influences this transition only by thermal smearing below the depinning temperature.[39] This low-temperature behavior can also be qualitatively understood by using a Lindemann criterion where only disorder-induced fluctuations $\overline{\langle u \rangle^2}$ are considered. Above the depinning temperature, however, thermal fluctuations change the renormalization-group flow equations. In a qualitative Lindemann analysis this behavior can only be obtained by the use of a Lindemann criterion analogously to Eq. (3) where both sorts of fluctuations act cooperatively.

If the dimensionality is further decreased and we consider a one-dimensional *single* vortex it is well known[1] that disorder even becomes irrelevant for $n>2$ where n is the number of components of the vortex displacement field. For the physical case of $n=2$ disorder is only marginally relevant, and it is the competition between quenched and thermal fluctuations that leads to an exponential increase in the crossover scale between the short-scale regime dominated by thermal fluctuations and the large-scale regime dominated by disorder fluctuations, the pinning length $L_c(T)$ [cf. Eq. (43) below]. In this sense, quenched disorder and thermal fluctuations always act cooperatively on single vortices. Therefore we expect the cooperative Lindemann criterion to eventually govern the physics in the very diluted regime where the thermal melting field b_m drops below the single-vortex pinning field b_{sv}.

We want to conclude this section by comparing the resulting phase diagrams if the criterion (3) based on cooperative action of quenched and thermal fluctuations is used or the criteria (2), (4), and (5) where quenched and thermal fluctua-

tions act independently. In Fig. 1 it is shown that naturally the stability boundary of the BrG phase is at slightly lower fields within the scenario of cooperatively acting fluctuations. At low T, when thermal fluctuations have no effect, and close to T_c both scenarios give identical results. The differences become most pronounced around the temperature T_x of three-phase coexistence in the second scenario of independently acting fluctuations. Based on the arguments presented before we will employ the approach of *independently* acting quenched and thermal fluctuations, i.e., the criteria (2), (4), and (5) throughout this paper which have also been used in Ref. 29 for BSCCO and which are supported by the melting theory presented in Ref. 9.

III. SINGLE-VORTEX LENGTH AND LINDEMANN CRITERION

Local Lindemann criteria of the form (2)–(5), which are probing fluctuations of changes in bond length $\Delta u(a,0)$ between nearest neighbors, can be reformulated in terms of the fluctuations of a single vortex line of a certain length which is set by the interactions with its nearest neighbors. This length scale is the so-called *single-vortex length* L_0 (in the notation of Ref. 1), which can be obtained within the elastic description of the FLL in terms of the displacement field $\mathbf{u}(\mathbf{r})$ with an elastic Hamiltonian that contains tilt, shear, and compression modes and associated elastic moduli c_{44}, c_{66}, and c_{11}, see for example Refs. 1 and 2. Over a wide range of parameters the vortex lattice is practically incompressible, $c_{11} \gg c_{66}$, such that transversal shear displacements are much larger than the longitudinal compression displacements at a given temperature or quenched randomness. Therefore, we can neglect the longitudinal displacement modes for what follows, and we consider a vortex line participating in a shear deformation on the scale of the vortex lattice unit cell $R=a$ perpendicular to the vortex line and on a scale L along the vortex line (we denote perpendicular scales by R and scales parallel to the vortex line by L). The corresponding wave vectors are $|\mathbf{K}|=K_{BZ}$ in the direction perpendicular to the vortex where $K_{BZ} \approx 2\sqrt{\pi}/a$ is the (circularized) Brillouin-zone radius and $q=1/L$ in the z direction along the vortex line. The single-vortex scale L_0 is determined by optimizing the sum of the tilt and shear energy of the vortex lattice unit cell $E_{tilt}+E_{shear}=c_{44}(K_{BZ},1/L)a^2u^2/L + c_{66}Lu^2$ with respect to the length L which gives

$$L_0 \simeq a \left(\frac{c_{44}(K_{BZ},1/L_0)}{c_{66}} \right)^{1/2} \simeq \left(\frac{\varepsilon_l(1/L_0)}{c_{66}} \right)^{1/2} \quad (6)$$

($\simeq$ is used if numerical prefactors are neglected), where we have to take into account the dispersion of the tilt modulus $c_{44}=c_{44}(K,q)$ whereas the shear modulus is approximately dispersion-free. Because $K \simeq 1/a$ represents the shortest wavelength $c_{44}(1/a,q) \simeq \varepsilon_l(q)/a^2$ is given by the single-vortex line tension $\varepsilon_l(q)$. The length scale L_0 sets the typical scale along the vortex line over which a single vortex can freely fluctuate relative to its neighbors. Fluctuations on larger scales are suppressed by the vortex interaction. This effective single-vortex model has also been called "cage

model''[25,29] because a vortex line is trapped in a hexagonal cage by the interaction with its nearest neighbors on scales larger than L_0. On scales smaller than L_0 the cage is large enough for the vortex line to freely fluctuate.

As the vortex lattice is essentially incompressible the elastic vortex lattice fluctuations are dominated by transversal shear and tilt modes which are described by the transversal part $G_T(\mathbf{K},q)$ of the elastic vortex lattice Green's function

$$G_T(\mathbf{K},q)=c_{66}K^2+c_{44}(K,q)q^2. \quad (7)$$

Tilt and shear contributions always enter the final results for thermal and disorder-induced displacement fluctuations through the elastic Green's function (7) as a rescaling of length scales in z direction shows.[3] Therefore the elastic Green's function (7) governs the scaling of tilt and shear contributions, and for a given wave vector K of shear deformation only tilt deformations with $q>K[c_{66}/c_{44}(K,q)]^{1/2}$ are accessible at comparable deformation energies both for thermal and disorder fluctuations. Thus the scaling of tilt and shear deformations due to Eq. (7) leads to the following result for displacements $\Delta u(L) \equiv \Delta u(0,L)=u(\mathbf{0},L)-u(\mathbf{0},0)$ and $\Delta u(\mathbf{R},0)=u(\mathbf{R},0)-u(\mathbf{0},0)$:

$$\langle \Delta u^2(\mathbf{R},0) \rangle_T = \langle \Delta u^2(0,L) \rangle_T,$$

$$\overline{\langle \Delta u^2(\mathbf{R},0) \rangle} = \overline{\langle \Delta u^2(0,L) \rangle}, \quad (8)$$

if the length R in direction perpendicular to the vortex lines and L in direction parallel to the vortex lines are related by $L \simeq R[c_{44}(1/R,1/L)/c_{66}]^{1/2}$. According to Eq. (6), the single-vortex length scale L_0 is defined such that $L=L_0$ and the vortex lattice spacing $R=a$ in the perpendicular direction form such a pair of length scales. Therefore we can use Eq. (8) to rewrite the Lindemann criteria (2)–(5) as

$$\langle \Delta u^2(a,0) \rangle_T = \langle \Delta u^2(0,L_0) \rangle_T,$$

$$\overline{\langle \Delta u^2(a,0) \rangle} = \overline{\langle \Delta u^2(0,L_0) \rangle}. \quad (9)$$

To calculate mean values of $\Delta u(L_0)=u(\mathbf{0},L_0)-u(\mathbf{0},0)$, however, we only need to know single-vortex properties on scales $L<L_0$ [the relative fluctuations of $\Delta u(L_0)$ are also identical to the total fluctuations u of a vortex of length $L=L_0$]. Hence, fluctuations of a single vortex up to the scale of the cage length are identical to relative fluctuations of two neighboring vortices. The local character of the Lindemann criteria (2)–(5) becomes even more obvious.

If the Lindemann criterion is formulated in terms of three characteristic energies as in Refs. 29 and 32 they also refer to the energies of a vortex fluctuation of wavelength L_0 parallel and wavelength a perpendicular to the vortex line. The typical thermal energy of such a fluctuation is T. The typical energy for a plastic deformation can be estimated by the elastic energy corresponding to a deformation with $u=c_L a$ which is $E_{pl} \simeq \varepsilon_l(1/L_0)c_L^2 a^2/L_0$. The typical pinning energy is estimated by the elastic energy corresponding to the typical pinning-induced displacement $u=\sqrt{\overline{\langle \Delta u(a,0) \rangle^2}}$ which is $E_{dis} \simeq \varepsilon_l(1/L_0)\overline{\langle \Delta u(a,0) \rangle^2}/L_0$. It becomes clear that the cri-

teria $T=E_{pl}$, $T+E_{dis}=E_{pl}$, $E_{dis}=E_{pl}$, and $T=E_{pin}$ are equivalent to the Lindemann criteria (2)–(5).

In the following we calculate the single-vortex length L_0 from Eq. (6). The result of this calculation will be

$$L_0 \simeq \begin{cases} \varepsilon a(1-b)^{-1/2} & \text{for } a < \lambda_{ab} \\ a\left(\dfrac{a}{\lambda_{ab}}\right)^{-3/4} \exp\left(\dfrac{1}{2}\dfrac{a}{\lambda_{ab}}\right) & \text{for } a > \lambda_{ab}, \end{cases} \quad (10)$$

where $b=B/B_{c2}=2\pi\xi_{ab}^2/a^2$ is the reduced magnetic induction, λ_{ab} is the magnetic penetration depth, and $\varepsilon=\lambda_{ab}/\lambda_c$ the anisotropy ratio of the type-II superconductor. Small logarithmic corrections are neglected in Eq. (10). In the dilute limit ($a > \lambda_{ab}$) and in the dense limit ($a < \lambda_{ab}$) very close to the upper critical field $1-b \ll 1$ the single-vortex length becomes very large. In both cases this is due to a softening of the lattice and a corresponding decrease in c_{66}, however for slightly different reasons. At low fields the vortex interaction decreases exponentially with increasing a/λ_{ab} leading to a softening, at extremely high fields softening is due to the effective increase of the magnetic penetration depth $\tilde{\lambda}_{ab}=\lambda_{ab}(1-b)^{-1/2}$ by the large normal cores of the vortices[2] and an effective decrease of the vortex-vortex interaction by a factor $(1-b)$.[40] The influence of the softening at high fields on the single-vortex length L_0 has been missed in Ref. 31 giving misleading results regarding the locus of the amorphization transition line for low-T_c materials such as NbSe where this effect becomes very important because melting and amorphization transition lines are both located in the vicinity of the upper critical field.

To calculate L_0 from Eq. (6) we need the shear modulus c_{66} and the single-vortex line tension $\varepsilon_l(q)$. The shear modulus c_{66} is given by[2,40]

$$c_{66} \approx \begin{cases} \dfrac{\varepsilon \epsilon_0}{4a^2}(1-b)^2 & \text{for } a < \lambda_{ab} \\ \dfrac{\varepsilon_0}{a^2}\sqrt{\dfrac{\pi}{6}}\left(\dfrac{a}{\lambda_{ab}}\right)^{3/2}\exp\left(-\dfrac{a}{\lambda_{ab}}\right) & \text{for } a > \lambda_{ab} \end{cases} \quad (11)$$

and exponentially decreasing in the dilute limit. The full expression for the dispersive vortex line tension is[2]

$$\varepsilon_l(q) \approx \frac{\varepsilon_0(1-b)}{2}\left[\varepsilon^2\ln\left(\frac{1}{K_{BZ}^2\xi_{ab}^2+\varepsilon^2\xi_{ab}^2q^2}\right) + \frac{(1-b)}{q^2\lambda_{ab}^2}\ln\left(1+\frac{q^2\lambda_{em}^2}{1+q^2u^2}\right)\right], \quad (12)$$

where $\varepsilon_0=(\Phi_0/4\pi\lambda_{ab})^2$ is the characteristic line energy of a vortex, and ξ_{ab} is the coherence length. The first term stems from the Josephson coupling between the line elements and is local whereas the second term originates from the electromagnetic interaction of line elements, and is thus strongly nonlocal. The scale

$$\lambda_{em}=\lambda_{ab}(1-b+K_{BZ}^2\lambda_{ab}^2)^{-1/2}\simeq\min\{\lambda_{ab}(1-b)^{-1/2},a\} \quad (13)$$

gives the length scale below which the nonlocality of the electromagnetic contribution sets in. It turns out to be relevant only in the dilute regime $a > \lambda_{ab}$ where $\lambda_{em}\approx\lambda_{ab}$. u is a typical displacement and the corresponding correction term in Eq. (12) is due to nonlinear elastic effects. Factors of $(1-b)$ in the expression (12) for the line stiffness result from extending the elastic theory for the FLL to higher magnetic fields $b > 0.25$ by replacing λ_{ab} by an effective magnetic penetration depth

$$\tilde{\lambda}_{ab}=\lambda_{ab}(1-b)^{-1/2} \quad (14)$$

that takes into account a renormalization due to the large normal cores of the vortices.[2] This also led to the replacement of ε_0 by $\tilde{\varepsilon}_0=\varepsilon_0(1-b)$ in Eq. (12). Using Eqs. (11) and (12) in Eq. (6) we obtain the above result (10) for the single-vortex length L_0.

The dispersive behavior of the single vortex line deserves some further attention. In the local limit (for wave vectors $q < 1/\lambda_{em}$) the stiffness becomes nondispersive and $\varepsilon_l \simeq \varepsilon_0[\varepsilon^2+(1-b)\lambda_{em}^2/\lambda_{ab}^2]$; the electromagnetic part dominates for all fields with $a > \varepsilon\lambda_{ab}$ where the stiffness takes on its isotropic value $\varepsilon_l \simeq \varepsilon_0$. In particular, the electromagnetic part governs the behavior in the whole dilute limit $a > \lambda_{ab}$. On the smallest scales $[q > 1/\varepsilon\tilde{\lambda}_{ab}=(1-b)^{1/2}/\varepsilon\lambda_{ab}]$, the Josephson contribution always dominates and we find an essentially nondispersive (we neglect a small logarithmically dispersive correction) but anisotropic stiffness $\varepsilon_l \simeq \varepsilon_0(1-b)\varepsilon^2$. On intermediate scales $1/\lambda_{em}<q<1/\varepsilon\tilde{\lambda}_{ab}$ the electromagnetic coupling dominates but it is reduced by dispersion until it is finally cut off by the Josephson contribution at $q \approx 1/\varepsilon\tilde{\lambda}_{ab}$. In this regime we find $\varepsilon_l \simeq \varepsilon_0(1-b)^2/q^2\lambda_{ab}^2$.

As can be seen from Eq. (10) the single-vortex length L_0 is always *smaller* than $\varepsilon\lambda_{ab}(1-b)^{-1/2}$ in the dense regime $a < \lambda_{ab}$. This means that in the whole dense regime the electromagnetic coupling is completely suppressed by the dispersion because L_0 is small enough that all fluctuations with $q < \varepsilon\tilde{\lambda}_{ab}$ are suppressed by the caging effect. Therefore, we need to consider large-scale fluctuations with $q < \varepsilon\tilde{\lambda}_{ab}$ only in the dilute limit where we can neglect factors of $(1-b)$ and set

$$\lambda_{em}\approx\lambda_{ab}. \quad (15)$$

Finally, this leads us to the following simplified expressions for the line stiffness which are justified if prefactors and logarithmic corrections are not crucial and valid only for the relevant fluctuations $q < 1/L_0$ which are not suppressed by the cage effect:

$$\varepsilon_l(q) \simeq \begin{cases} a < \lambda_{ab}: & \varepsilon_0(1-b)\varepsilon^2 \\[2ex] a > \lambda_{ab}: & \begin{cases} \varepsilon_0 & \text{for } q < \dfrac{1}{\lambda_{ab}} \\[2ex] \dfrac{\varepsilon_0}{q^2 \lambda_{ab}^2} & \text{for } \dfrac{1}{\lambda_{ab}} < q < \dfrac{1}{\varepsilon \lambda_{ab}} \\[2ex] \varepsilon_0 \varepsilon^2 & \text{for } q > \dfrac{1}{\varepsilon \lambda_{ab}}. \end{cases} \end{cases} \tag{16}$$

IV. SINGLE-VORTEX FLUCTUATIONS AND ELECTROMAGNETIC COUPLING

As already pointed out we can use Eq. (9) to calculate the averages in the Lindemann criteria (2)–(5) by considering single-vortex fluctuations up to the scale L_0 set by the vortex interaction. As the simplified expression (16) shows there are no further complications from nonlocal couplings in the dense regime $a < \lambda_{ab}$ because the essentially nondispersive Josephson coupling governs the behavior up to the scale L_0 in this regime.

This, however, changes if the dilute limit $a > \lambda_{ab}$ is considered where competing effects of Josephson and electromagnetic coupling between vortex elements have to be taken into account as Eq. (16) shows. The effects for single-vortex fluctuations due to temperature and quenched disorder are discussed in detail elsewhere.[41] For a self-contained discussion we will present here the main results.

Due to the competing nonlocal electromagnetic and local Josephson coupling there is a window of wave vectors $1/\lambda_{ab} < q < 1/\varepsilon\lambda_{ab}$ in the dilute limit $a > \lambda_{ab}$ where the line stiffness is strongly dispersive with $\varepsilon_l(q) \propto q^{-2}$, see Eq. (16). In the limit of a very weak Josephson coupling $\varepsilon \to 0$ the dispersion of the electromagnetic contribution persists down to the shortest length scale, which is then set by the layer distance d. For the fluctuation behavior in the dilute limit the largest possible wave vector showing q^{-2} dispersion is important. In a layered material this is $q_d \simeq 1/\max\{d, \varepsilon\lambda_{ab}\}$ and we introduce a corresponding *dispersion length scale*

$$L_d = \max\{d, \varepsilon\lambda_{ab}\} = \lambda_{ab}\max\{\varepsilon_d, \varepsilon\}, \tag{17}$$

where

$$\varepsilon_d = \frac{d}{\lambda_{ab}} \tag{18}$$

is an effective *layered anisotropy* of the material. For the short-scale fluctuations it is important to distinguish between two classes of superconductors depending on the strength of the Josephson coupling or the size of ε. Superconductors with a *strong* Josephson coupling $\varepsilon > \varepsilon_d$ have $L_d \simeq \varepsilon\lambda_{ab}$; YBCO falls into this class and of course all low-T_c materials such as NbSe without layered structures. On the other hand, superconductors with a *weak* Josephson coupling $\varepsilon < \varepsilon_d$ have $L_d \simeq d$. But it has to be noted that even if $\varepsilon < \varepsilon_d$ at $T = 0$ the Josephson coupling becomes strong above a temperature

$$t_d = 1 - (\varepsilon/\varepsilon_d)^2 \tag{19}$$

because $\varepsilon_d \propto (1-t)$, where $t = T/T_c$ is the reduced temperature. For typical parameters for BSCCO, $\varepsilon \approx 1/200$, $d \approx 15$ Å, $\lambda_{ab} \approx 2000$ Å, and $T_c \approx 100$ K one finds that BSCCO has a weak Josephson coupling at low temperatures but the Josephson coupling becomes strong above $T_d \approx 36$ K.

Considering only fluctuations with wave vectors $1/\lambda_{ab} < q < q_d$ one can show that due to the predominantly electromagnetic coupling each vortex segment of length λ_{ab} effectively *decouples* into small segments of length L_d that fluctuate independently in a harmonic potential.[42] Therefore, the vortex line becomes very soft with respect to fluctuations on the short scale L_d. This holds for thermal fluctuations as well as for fluctuations due to pinning. In particular, this leads both for thermal and for fluctuations from quenched point disorder to a breakdown of scaling in the displacement correlations. For $L > L_d$ displacements $\langle \Delta u^2(L) \rangle_T$ or $\overline{\langle \Delta u^2(L) \rangle}$ essentially do *not* grow over a certain regime of length scales (neglecting eventual weak logarithmic corrections). Furthermore, on scales $L > \lambda_{ab}$, $\langle \Delta u^2(L) \rangle_T$ or $\overline{\langle \Delta u^2(L) \rangle}$ can be calculated in the conventional way using the isotropic stiffness $\varepsilon_l(q) \simeq \varepsilon_0$ but short-scale contributions $\langle \Delta u^2(L_d) \rangle_T$ and $\overline{\langle \Delta u^2(L_d) \rangle}$ have to be taken explicitly into account. Specifically, we find for $L = L_0$ (the following equation holds analogously for thermal averages $\langle \cdots \rangle_T$)

$$\overline{\langle \Delta u^2(L_0) \rangle}$$
$$\simeq \begin{cases} \overline{\langle \Delta u^2(L_0) \rangle_\varepsilon} & \text{for } d < L_0 < \varepsilon\lambda_{ab} \\[1ex] \overline{\langle \Delta u^2(L_d) \rangle} & \text{for } L_d < L_0 < \lambda_{ab} \\[1ex] \overline{\langle \Delta u^2(L_0) \rangle_i} + \overline{\langle \Delta u^2(L_d) \rangle} & \text{for } L_0 > \lambda_{ab}, \end{cases} \tag{20}$$

where the subscript "ε" implies that only large wave vectors $q > \varepsilon\lambda_{ab}$ are integrated over and thus the average is performed using the anisotropic stiffness $\varepsilon_l(q) \simeq \varepsilon_0\varepsilon^2$ and analogously the subscript "i" implies that only small wave vectors $q < \lambda_{ab}$ are integrated over and thus the average is performed using the local limit of Eq. (16) where the stiffness is isotropic $\varepsilon_l \simeq \varepsilon_0$.

According to the Lindemann criteria (2)–(5) in conjunction with Eq. (9) the vortex phase diagram is determined by the displacement fluctuations of a single-vortex on scales $L < L_0$. From Eq. (20), the structure of the phase diagram with regard to the dominant scale of these single-vortex fluctuations becomes clear, see Fig. 2. In the dense regime $a < \lambda_{ab}$ the essentially nondispersive anisotropic Josephson part of $\varepsilon_l(q)$ is always dominating. Then the largest scale L_0 in the cage model is the dominant scale of fluctuations as in the first line of Eq. (20) but we have to include possible high-field corrections and use $\varepsilon_l(q) \simeq \varepsilon_0(1-b)\varepsilon^2$ in the dense limit. Evaluation of the Lindemann criteria will show that this produces the upper branches of both the melting and the amorphization transition line in the regime $a < \lambda_{ab}$ of the B-T plane, see Fig. 2.

In the dilute limit $a > \lambda_{ab}$ the situation becomes more complicated because L_0 grows exponentially with a, see Eq. (10), and thus $L_0 > \lambda_{ab}$ essentially in the whole dilute limit. Then effects from the nonlocal electromagnetic coupling be-
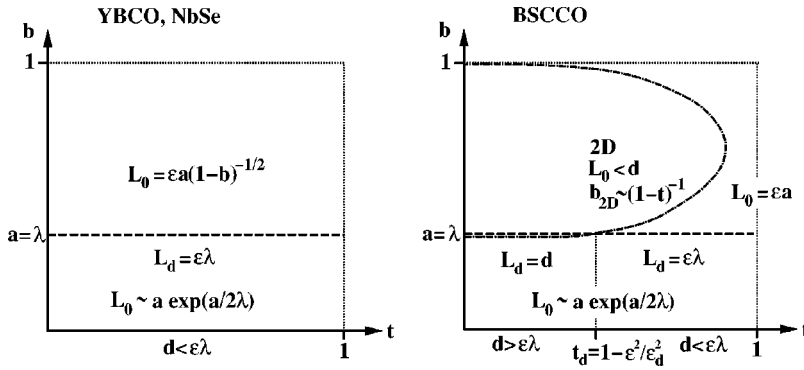
FIG. 2. Schematic diagrams in the b-t plane (the dilute regime is enlarged) showing the dominant scales for displacement fluctuations of a single-vortex of length L_0. For YBCO and NbSe fluctuations on the largest scale L_0 dominate in the dense regime and determine the upper branches of the melting and order-disorder transition lines. BSCCO exhibits quasi-2D behavior in large parts of the dense regime. Fluctuations on the exponentially large scale L_0 also determine the lower branches of transition lines deep in the dilute regime for YBCO, NbSe, and BSCCO. The continuation of the upper branches of the transition lines into the dilute regime, however, is determined by fluctuations on the scale L_d; for YBCO and NbSe $L_d = \varepsilon \lambda_{ab}$ whereas for BSCCO $L_d = d$ at low temperatures.

come relevant and according to Eq. (20) fluctuations from two scales—L_0 and $L_d = \max\{d, \varepsilon \lambda_{ab}\}$—are dominant. Evaluation of the Lindemann criteria shows that fluctuations on the scale L_d give the continuation of the upper branch of both the melting and the amorphization transition line into the dilute regime whereas fluctuations on the exponentially large scale L_0 give the lower branches of both transition lines, see Fig. 2. Thus the nonlocal electromagnetic coupling is responsible for the typical phase diagrams with reentrant liquid or amorphous vortex phases that we will find, see Figs. 3, 6, and 7. Experimentally, lower branches of neither the melting nor the order-disorder transition line could be observed so far in the dilute regime. Therefore we will focus on the upper branches throughout this paper. Given the results in Ref. 41, a calculation of the lower branches is in principle straightforward but actually very involved as the full fluctuation behavior including the interplay of thermal and quenched fluctuations over all length scales is very diverse.

As the previous discussion showed, in order to calculate the upper branches of the transition lines, we only need to consider single-vortex fluctuations with the nondispersive anisotropic stiffness $\varepsilon_l(q) \simeq \varepsilon_0(1-b)\varepsilon^2$ from the Josephson coupling as long as we have strong Josephson coupling with $L_d = \varepsilon \lambda_{ab}$ as for YBCO and NbSe. Only for the upper branch of the transition lines in the dilute limit for BSCCO with a weak Josephson coupling dispersion becomes crucial, and we have to take into account fluctuations on the scale of the layer spacing $L_d = d$. This means we have to consider fluctuations of a single pancake vortex relative to its neighbors in adjacent layers.

Quasi-2D behavior of the vortex lattices becomes relevant for melting processes as soon as $L_0 < d$ when the tilt energy can be neglected against the shear energy on the scale of one layer spacing d. The crossover condition $L_0 < d$ is fulfilled for $b > b_{2D}$ above the *2D crossover field*
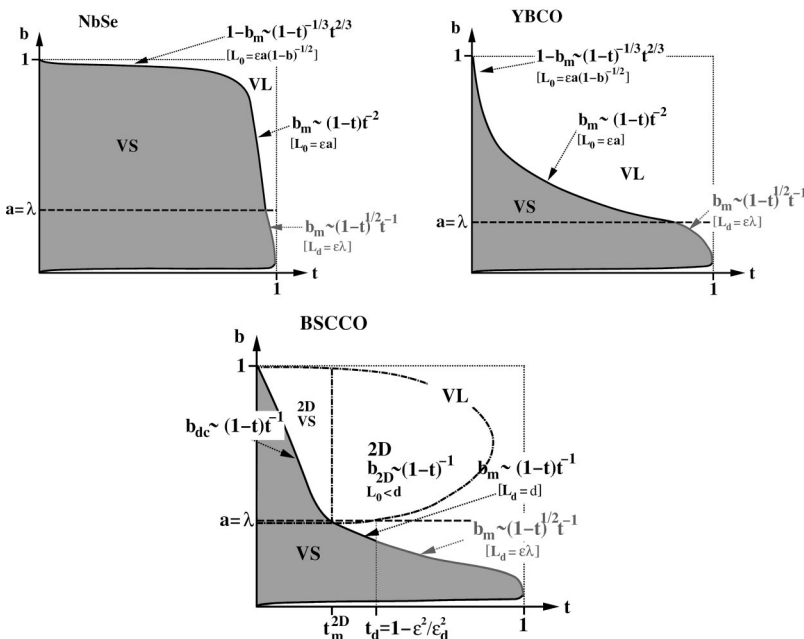

FIG. 3. Schematic phase diagrams for thermal melting of the vortex solid (VS) into a vortex liquid (VL) in the absence of quenched disorder for NbSe, YBCO, and BSCCO. For BSCCO above the crossover field b_{2D} there is a decoupling into a 2D VS prior to melting. (The dilute regime is enlarged, the reentrance at very low fields is shown for completeness but not discussed in the text.)

$$b_{2D} \simeq \frac{2\pi}{\kappa^2} \max \left\{ \frac{\varepsilon^2}{\varepsilon_d^2}(1-b)^{-1}, 1 \right\}, \qquad (21)$$

where we used Eq. (10) and neglected a logarithmic correction.[1] $\kappa = \lambda_{ab}/\xi_{ab}$ is the Ginsburg-Landau parameter. For a strong Josephson coupling $\varepsilon > \varepsilon_d$ the crossover field is in the dense regime and has a temperature dependence $b_{2D}(1-b_{2D}) \propto (1-t)^{-1}$. From Eq. (10) one derives that for $\varepsilon > d/5\xi_{ab}$ we *always* have $L_0 > d$ and there is no crossover to quasi-2D behavior. This condition is actually fulfilled for YBCO with typical parameters $\varepsilon \approx 1/5$, $d \approx 12$ Å, and $\xi_{ab} \approx 15$ Å. Therefore we will exclude the possibility of 2D behavior for YBCO in our subsequent discussions of melting and order-disorder transitions. For a weak Josephson coupling $\varepsilon < \varepsilon_d$ the 2D crossover field is approximately equal to (actually slightly below) the field $b = 2\pi/\kappa^2$ at which $a = \lambda_{ab}$, i.e., the boundary between the dilute and dense regime. This means for a weak Josephson coupling, e.g., in BSCCO below $T_d \approx 36$ K, the vortex lattice melting shows quasi-2D behavior in the whole dense limit. It is expected that as soon as the melting or the amorphization transition line intersects the line $b_{2D}(t)$ the character of the melting or amorphization process changes from 3D linelike to quasi-2D and decoupling of the FLL happens prior to the melting, which is then a 2D melting transition.

However, it has been a long-standing question[7] whether already the dominance of fluctuations on the scale $L_d = d$ given by the layer spacing (for weak Josephson coupling, e.g., in BSCCO) in the dilute regime leads to a qualitatively different melting transition. Because these decoupling quasi-2D fluctuations dominate the mean-square displacements in the Lindemann criterion for melting one can argue that melting and decoupling happen in a single transition or, in other words, that the FLL melts or becomes amorphous *by decoupling*. The argument against this point of view is that $L_0 > d$ still holds and pancake vortex lattices in different layers are interacting logarithmically.[42] For the thermal melting transition it has been convincingly demonstrated in Ref. 43 that even in the absence of a Josephson coupling $\varepsilon = 0$ there is still a 3D lattice melting at low magnetic fields $B < B_{2D}$. However, this subtle issue is beyond the scope of the Lindemann criteria employed in this paper. For the case of the amorphization transition in the presence of disorder the analogous question is still unanswered.

A two-dimensional BrG phase has been shown to be *always* unstable with respect to dislocation formation in the presence of disorder[44] such that the decoupling transition leads directly to a 2D amorphous VG if amorphization does not happen prior to decoupling. At this point it should also noted that a Lindemann-like criterion analogous to Eq. (4) would give the incorrect result regarding the instability of the 2D BrG phase as it would predict the existence of an amorphization transition and thus of a quasiordered 2D BrG phase below a critical disorder strength.

Figure 2 summarizes the findings of this section regarding the relevant length scales for the fluctuations causing melting or amorphization for the three exemplary materials we want to study in this paper. YBCO has a strong Josephson cou-

pling and $L_d = \varepsilon \lambda_{ab}$, BSCCO a weak Josephson coupling and thus $L_d = d$ for temperatures $T < T_d$, and in the low-T_c material NbSe there is no layered structure at all (formally corresponding to $\varepsilon_d \approx 0$) and $L_d = \varepsilon \lambda_{ab}$.

V. THERMAL MELTING

First we want to briefly recapitulate the calculation of thermal melting curves in the absence of disorder according to the Lindemann criterion (2) or the equivalent criterion

$$\langle \Delta u^2(L_0) \rangle_T = c_L^2 a^2 \qquad (22)$$

formulated in terms of displacement fluctuations of a single-vortex on scales $L < L_0$ using Eq. (9), to which we apply our results of the preceding section for the length scales of the relevant fluctuations causing melting. For thermal melting we will reproduce the well-known results of Ref. 6 for anisotropic materials and Ref. 7 for strongly layered materials. We rederive these results as part of the complete phase diagram and to demonstrate the simplicity and correctness of the present approach. The results are summarized in Fig. 3 for NbSe, YBCO, and BSCCO.

A. YBCO and NbSe

YBCO and NbSe are both anisotropic type-II superconductors and have qualitatively similar melting curves as long as the layered structure of YBCO can be neglected. Fluctuations are larger in the high-T_c material YBCO due to the increased transition temperatures ($T_c \approx 90$ K for YBCO and $T_c \approx 6$ K for NbSe) and lower coherence lengths ($\xi_{ab} \approx 20$ Å in YBCO and $\xi_{ab} \approx 100$ Å in NbSe) which lead to a *Ginsburg number*[1]

$$\mathrm{Gi} = \frac{1}{8} \left(\frac{T_c}{\varepsilon \varepsilon_0 \xi_{ab}} \right)^2 \qquad (23)$$

which is $\mathrm{Gi} \approx 1.5 \times 10^{-2}$ for YBCO but much smaller $\mathrm{Gi} \approx 1.7 \times 10^{-6}$ in NbSe. Therefore, the vortex lattice melting in the low-T_c material NbSe takes place only at high fields in the vicinity of H_{c2}, see Fig. 3.

As pointed out in Sec. IV, the Josephson coupling dominates throughout the dense regime $a < \lambda_{ab}$ and thus we use the anisotropic line stiffness $\varepsilon_l(1/L_0) \simeq \varepsilon_0(1-b)\varepsilon^2$ and $L_0 \simeq \varepsilon a(1-b)^{-1/2}$ from Eq. (10) to obtain

$$\langle \Delta u^2(L_0) \rangle_T \simeq \frac{T L_0}{\varepsilon_l} \simeq a^2 \left(\frac{b}{2\pi} \right)^{1/2} (1-b)^{-3/2} \frac{T}{\varepsilon \varepsilon_0 \xi_{ab}}. \qquad (24)$$

With the Lindemann criterion (22) this gives for the upper branch $b_m(t)$ of the melting line the well-known result[6,1]

$$\frac{b_m}{(1-b_m)^3} \simeq \frac{\pi}{4} c_L^4 \mathrm{Gi}^{-1}(1-t)t^{-2}. \qquad (25)$$

For $b \ll 1$ the factors $1-b$ can be neglected and $b_m \propto (1-t)t^{-2}$ or $B_m \propto (1-t)^2 t^{-2}$. Close to the upper critical field for $1-b \ll 1$, this yields

$$1 - b_m \simeq \left(\frac{\pi}{4}\right)^{-1/3} c_L^{-4/3} \text{Gi}^{1/3} (1-t)^{-1/3} t^{2/3}. \quad (26)$$

If the upper branch of the melting line is continued into the dilute limit $a > \lambda_{ab}$ fluctuations on the scale L_d dominate the expectation value in the Lindemann criterion (22), $\langle \Delta u^2 (L_0) \rangle_T \simeq \langle \Delta u^2 (L_d) \rangle_T$. YBCO and NbSe have a strong Josephson coupling and thus $L_d = \varepsilon \lambda_{ab}$. On the scale $\varepsilon \lambda_{ab}$, we use again the anisotropic line stiffness $\varepsilon_l (1/\varepsilon \lambda_{ab}) \simeq \varepsilon_0 \varepsilon^2$ and get

$$\langle \Delta u^2 (\varepsilon \lambda_{ab}) \rangle_T \simeq \frac{T \varepsilon \lambda_{ab}}{\varepsilon_l} \simeq a^2 \frac{b}{2\pi} \kappa \frac{T}{\varepsilon \varepsilon_0 \xi_{ab}}. \quad (27)$$

Thus the Lindemann criterion gives the upper branch $b_m (t)$ of the melting line in the dilute limit as

$$b_m \simeq \frac{\pi}{\sqrt{2}} c_L^2 \kappa^{-1} \text{Gi}^{-1/2} (1-t)^{1/2} t^{-1} \quad (28)$$

or $B_m \propto (1-t)^{3/2} t^{-1}$.[7]

B. BSCCO

The strongly layered BSCCO has a weak Josephson coupling at temperatures below $T_d \approx 36$ K. The upper branch of the melting line should intersect the 2D crossover line $b_{2D}(t)$ around the 2D melting temperature of a superconducting layer $T_m^{2D} \approx d\varepsilon_0/70$.[1] Taking again $d \approx 15$ Å and $\lambda_{ab} \approx 2000$ Å as typical parameters for BSCCO, one finds $T_m^{2D} \approx 10$ K which is well below T_d. This means that at the temperature T_m^{2D} the 2D crossover line is at the boundary to the dense regime, see Eq. (21), such that the upper branch of the 3D melting line lies entirely in the dilute regime, see Fig. 3.

In the case of a weak Josephson coupling at $T=0$ another phase diagram for the 3D thermal melting is possible if d and ε are such that $T_m^{2D} > T_d$. In this case the upper branch of the melting line will enter the dense regime before the melting transition turns into 2D melting, and the phase diagram looks qualitatively similar to that of YBCO. But for clarity of presentation we will limit the discussion here to the situation $T_m^{2D} < T_d$ that arises for a realistic choice of parameters for the BSCCO material.

In the dilute regime, BSCCO exhibits a behavior distinct from YBCO or NbSe due to its weak Josephson coupling or $L_d = d$. At the upper branch of the melting line fluctuations on the scale of the layer spacing $L_d = d$ dominate the mean-square displacement in Eq. (22) due to the nonlocal electromagnetic coupling as discussed in Sec. IV, i.e., $\langle \Delta u^2 (L_0) \rangle_T \simeq \langle \Delta u^2 (d) \rangle_T$. To calculate $\langle \Delta u^2 (d) \rangle_T$ on the scale of the layer distance, the fluctuations of single pancakes have to be considered. This can be done in much more microscopic detail (see for example Ref. 42) but for our purposes we can consider a single pancake coupled to the pancakes in adjacent layers by a harmonic potential $\varepsilon_l (1/d) \Delta u^2/d$, and use $\varepsilon_l (1/d) \simeq \varepsilon_0 \varepsilon_d^2$ from Eq. (16) (where we neglected logarithmic corrections[42] in u). We obtain

$$\langle \Delta u^2 (d) \rangle_T \simeq \frac{Td}{\varepsilon_l (1/d)} \simeq a^2 \frac{b\kappa^2}{2\pi} \frac{T}{\varepsilon_0 d} \quad (29)$$

and the Lindemann criterion gives the upper branch $b_m (t)$ of the melting line for BSCCO in the dilute limit as

$$b_m (t) \simeq \sqrt{2} \pi c_L^2 \kappa^{-2} \text{Gi}_{2D}^{-1} (1-t) t^{-1} \quad (30)$$

or $B_m (t) \propto (1-t)^2 t^{-1}$,[7] where we used the 2D Ginsburg number $\text{Gi}_{2D} = 2\text{Gi}^{1/2} \kappa^{-1} \varepsilon/\varepsilon_d \approx T_c/100 T_m^{2D}$.[1] For BSCCO with $T_c \approx 100$ K the 2D Ginsburg number is $\text{Gi}_{2D} \approx 0.096$. For low temperatures $t \ll 1$, we can rewrite Eq. (30) to get the melting temperature as function of field b,

$$T_m (b) \simeq T_m^{2D} 70 c_L^2 \frac{2\pi}{b\kappa^2} \quad (31)$$

showing that the transition approaches indeed the 2D melting transition of a layer upon intersecting $b_{2D} \approx 2\pi/\kappa^2$ (if we choose $c_L \approx 1/\sqrt{70}$), see Fig. 3.

For temperatures $T < T_m^{2D}$ the 3D vortex solid first undergoes a decoupling transition at a field b_{dc} into a 2D vortex solid which undergoes a 2D melting transition at T_m^{2D}. If this decoupling transition is also described by a Lindemann criterion of the form

$$\langle \Delta u^2 (0, d) \rangle_T = c_L^2 a^2 \quad (32)$$

as suggested in Refs. 7 and 48, we will get the same formulas (30) and (31) for the decoupling transition line $b_{dc}(t)$ or alternatively $T_{dc}(b)$, which is thus the continuation of the 3D melting line into the 2D regime, see Fig. 3.

VI. PINNING OF SINGLE VORTICES

Before addressing the BrG stability boundaries by using the Lindemann criterion (4) we want to discuss different pinning regimes depending on the strength of the frozen disorder. We consider a single elastic vortex line with stiffness $\varepsilon_l (q)$ in a quenched disorder potential $V(z, \mathbf{u})$ with a Gaussian distribution, zero mean, and short-range correlations in all directions,

$$\overline{V(z, \mathbf{u}) V(z', \mathbf{u}')} = \gamma \xi_{ab}^4 \delta(z - z') \Delta_{\xi_{ab}}(\mathbf{u} - \mathbf{u}'). \quad (33)$$

The parameter γ gives the strength of the quenched disorder and is temperature dependent.[1] This temperature dependence due to the microscopic pinning mechanism will be discussed further below. Usually, we consider point disorder correlations of a short range ξ_{ab} given by the size of the vortex cores with and an integrable disorder correlator $\Delta_{\xi_{ab}}(\mathbf{u})$ that we normalize such that $\int d^2 \mathbf{u} \Delta_{\xi_{ab}}(\mathbf{u}) = 1$. Then we can approximate $\Delta_{\xi_{ab}}(\mathbf{u}) \approx \delta_{\xi_{ab}}(\mathbf{u})$ by a δ function of range ξ_{ab}. For single-vortex pinning, however, the correlation function $\Delta_{\xi_{ab}}(\mathbf{u})$ can be weakly (logarithmically) nonintegrable. This will only affect the thermal depinning behavior.[45]

A convenient *pinning strength parameter* δ (see Ref. 1) is defined by the ratio of the mean-square pinning energy $E_{pin}^2 (\xi_c) \simeq \gamma \xi_{ab}^2 \xi_c$ for a small line element of length $L \simeq \xi_c$

and with typical displacement $u \simeq \xi_{ab}$ and the square of the corresponding tilt energy $E_{tilt}(\xi_c) \simeq \varepsilon_0 \varepsilon^2 \xi_{ab}^2/\xi_c \simeq \varepsilon_0 \xi_c$,

$$\frac{\delta}{\varepsilon} = \frac{\gamma \xi_{ab}^2 \xi_c}{(\varepsilon_0 \xi_c)^2}. \tag{34}$$

It should be noted that this expression has *no* correction factors $(1-b)$ at high fields because $\gamma \propto f_{pin}^2 \propto \varepsilon_0^2$, where f_{pin} is the pinning force exerted by a single point defect;[1,31] therefore corrections due to the replacement $\varepsilon_0 \rightarrow \tilde{\varepsilon}_0 = \varepsilon_0(1-b)$ in Eq. (34) cancel.

In a layered material one can consider the analogous energies for a segment of length $L \simeq d$, i.e., the mean-square pinning energy $E_{pin}^2(d) \simeq U_p^2$ with the *pancake pinning energy*

$$U_p = (\gamma \xi_{ab}^2 d)^{1/2} \tag{35}$$

and the square of the corresponding tilt energy $E_{tilt}(d) \simeq \varepsilon_l(1/d)\xi_{ab}^2/d \simeq \varepsilon_0(\varepsilon^2 + \varepsilon_d^2)\xi_{ab}^2/d$, see Eq. (16). Using this we define an analogous *layered pinning strength parameter* δ_d as

$$\delta_d = \frac{U_p^2}{[\varepsilon_0(\varepsilon^2 + \varepsilon_d^2)\xi_{ab}^2/d]^2}. \tag{36}$$

From the definitions (34) and (36) it is clear that collective pinning theory applies to weak pinning $\delta/\varepsilon \ll 1$ and $\delta_d \ll 1$. Whereas the former condition is usually fulfilled both in low-T_c materials such as NbSe and anisotropic HTSC's such as YBCO, the latter condition is violated in layered HTSC's with strong disorder, e.g., in BSCCO. We will call pinning with $\delta_d > 1$ *strong pinning*. Experimental estimates for the pinning strength can be obtained from measurements of the (single-vortex) critical current j_c using the relation $j_c \simeq j_0(\delta/\varepsilon)^{2/3}$, where $j_0 \simeq c\varepsilon_0/\xi_{ab}\Phi_0$ is the depairing current.[1] Due to their larger anisotropy and the intrinsic doping typical values for the pinning parameter δ/ε are usually higher in the high-T_c materials YBCO and BSCCO. Throughout this paper we assume values $\delta/\varepsilon \approx 10^{-2}$ for YBCO (corresponding to $j_c \approx 10^7$ A cm^{-2}) and much smaller values $\delta/\varepsilon \approx 10^{-9}$ for the low-T_c material NbSe (corresponding to $j_c/j_0 \sim 10^{-6}$, see Ref. 47), both well in the weak pinning regime. For BSCCO we find indeed strong pinning $\delta_d \approx 10^4 \gg 1$ using an estimate $U_p \approx 10$ K (these values correspond to $\delta/\varepsilon \approx 0.03$).

There are two basic microscopic pinning mechanisms, δl pinning from variations in the mean free path and δT_c pinning from variations in T_c, which give rise to a different temperature dependence of δ/ε. Without going into details here it is found[1,31] that

$$\delta \propto (1-t)^{3/2} \quad (\delta l \text{ pinning}), \tag{37}$$

$$\delta \propto (1-t)^{-1/2} \quad (\delta T_c \text{ pinning}). \tag{38}$$

Whereas for high-T_c materials (YBCO, BSCCO) the thermal smearing of the pinning energy landscape above the depinning temperature T_{dp} is much more important because it sets

in at much lower temperatures ($T_{dp} \ll T_c$), the temperature dependence through the microscopic parameters of δ plays an important role in low-T_c materials (NbSe) where the depinning temperature essentially coincides with T_c.

A. Weak collective pinning

Within weak collective pinning theory the central crossover length for a single-vortex is the *collective pinning or Larkin length L_c* which is defined as the length scale at which $\overline{\langle \Delta u(L_c) \rangle^2} = \xi_{ab}^2$ at low temperatures. On smaller scales perturbation theory applies and the disorder potential can be expanded into random forces (RF). In this regime the roughness exponent is $\zeta_{RF} = 3/2$, i.e., $\overline{\langle \Delta u(L) \rangle^2} \propto L^3$. Segments longer than L_c, on the other hand, explore many almost degenerate minima of the pinning energy landscape. In this so-called random manifold (RM) regime we use the estimate $\zeta_{RM} \approx 5/8$ for the roughness exponent.[49,50] Note that slightly different estimates for ζ_{RM} have been used in previous Lindemann analysis; different estimates are discussed theoretically in Ref. 50. References 26 and 27 implicitly use $\zeta_{RM} \approx 1/2$ (from a variational replica approach), Refs. 28, 29, 31, and 32 use $\zeta_{RM} \approx 3/5$, and Refs. 25 and 30 use $\zeta_{RM} \approx 5/8$ which gives practically identical results to $\zeta_{RM} \approx 3/5$. As pointed out in Sec. IV we only need to consider single-vortex fluctuations with the nondispersive anisotropic Josephson stiffness and fluctuations of single pancakes on the scale d if we are only interested in the upper branch of the order-disorder transition between BrG and amorphous VG phase.

For pinned single vortex lines with the anisotropic Josephson stiffness we have at low temperatures the usual anisotropic collective pinning length[1]

$$L_c \simeq \varepsilon \xi_{ab} \left(\frac{\delta}{\varepsilon} \right)^{-1/3} \tag{39}$$

which has *no* correction factors $(1-b)$ at high fields exactly like δ/ε. The displacement fluctuations are given by

$$\overline{\langle \Delta u(L) \rangle^2} \simeq \xi_{ab}^2 \left(\frac{L}{L_c} \right)^3 \quad \text{for } L < L_c, \tag{40}$$

$$\overline{\langle \Delta u(L) \rangle^2} \simeq \xi_{ab}^2 \left(\frac{L}{L_c} \right)^{5/4} \quad \text{for } L > L_c. \tag{41}$$

There are two important crossovers upon increasing the disorder strength, the crossover from bundle pinning to single-vortex pinning[1] if L_c decreases below the single-vortex length L_0 set by the interaction between vortices and the crossover from weak collective to strong pinning if L_c drops below the layer spacing d and we have to consider the strong pinning of individual pancake vortices.[41]

At higher temperatures the disorder gets effectively weakened by thermal fluctuations within the pinning energy landscape as soon as $\langle \Delta u^2(L_c) \rangle_T = \xi_{ab}^2$. This happens at the anisotropic depinning temperature

$$T_{dp} \simeq \varepsilon \varepsilon_0 \xi_{ab} \left(\frac{\delta}{\varepsilon} \right)^{1/3} \tag{42}$$

above which an exponential increase of the pinning length sets in[1,45]

$$L_c(T) \simeq L_c \frac{T_{dp}}{T} e^{C(T/T_{dp})^\alpha} \tag{43}$$

with a numerical factor C and an exponent α. For point disorder with an integrable disorder correlation function $\Delta_{\xi_{ab}}(\mathbf{u})$ one finds $\alpha = 3$,[1,45] and the numerical factor $C = 32/\pi$ has been determined in Ref. 46. For a weakly non-integrable function $\Delta_{\xi_{ab}}(\mathbf{u})$, however, as in the case of single-vortex pinning it has been shown in Ref. 45 that the exponential growth of the pinning length due to thermal smearing is slightly modified in the temperature range $T_{dp} < T < T_{dp} \ln \kappa$ where an exponent $\alpha = 1$ is found whereas the precise value of C is unknown. The exponent $\alpha = 3$ as for an integrable disorder correlator only holds above the temperature $T_{dp} \ln \kappa$. The displacement fluctuations for $L > L_c(T)$ become

$$\overline{\langle \Delta u(L) \rangle^2} \simeq \xi_{ab}^2 \left(1 + \frac{T}{T_{dp}} \frac{L_c(T)}{L_c(0)} \right) \left(\frac{L}{L_c(T)} \right)^{5/4}. \tag{44}$$

Note that thermal depinning plays no role in low-T_c materials where $\varepsilon \varepsilon_0 \xi_{ab} \sim 1000$ K at $T=0$, and the depinning temperature practically coincides with T_c if the temperature dependence of the microscopic parameters λ_{ab} and ξ_{ab} is taken into account and T_{dp} is calculated self-consistently from Eq. (42).

B. Single vortex versus bundle pinning

For $L_0 < L_c$ pinned vortices on the scale of the pinning length are already interacting and the collectively pinned objects are vortex bundles rather than single vortices.[1] The regime $L_0 < L_c$ is called *bundle pinning* regime. For our purposes bundle pinning simply means that on the scale of the single-vortex length, single-vortex displacements are still treated correctly by the perturbative RF regime (40). On the other hand, for $L_0 > L_c$ the pinned objects on the scale of the pinning length are single-vortex lines rather than bundles. The regime $L_0 > L_c$ is therefore called *single-vortex pinning* regime. In this regime the RF regime does no longer apply on the single-vortex scale L_0 but we rather have to apply the findings (41) for the RM regime. For the following discussion of different materials it is crucial to know the *single-vortex pinning field* b_{sv} where the crossover between single-vortex and bundle pinning happens within the pinning diagram in the b-δ plane. For our purposes, we can focus the discussion on the dense regime $a < \lambda_{ab}$, in the dilute regime single-vortex pinning is dominant because interactions become exponentially weak. At $T=0$ the condition $L_0 = L_c$ for b_{sv} gives

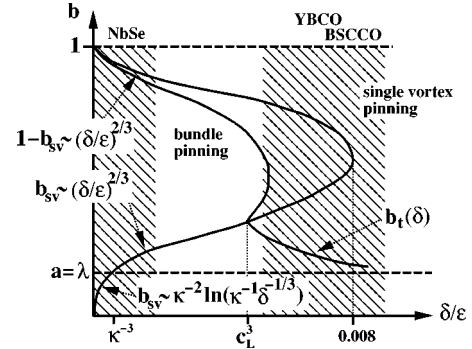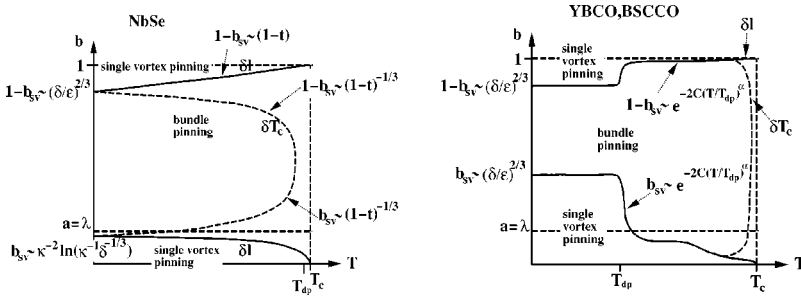$$b_{sv}(1 - b_{sv}) \simeq 2\pi \left(\frac{\delta}{\varepsilon} \right)^{2/3} \tag{45}$$

FIG. 4. Schematic pinning diagram in the b-δ plane showing the single-vortex pinning field b_{sv} at low temperatures (the dilute regime is enlarged). Due to their larger anisotropy typical values for the pinning parameter δ/ε are usually higher in the high-T_c materials YBCO and BSCCO and lie in the single-vortex pinning regime (right hatched region). They are lower in the low-T_c materials such as NbSe and lie typically in the bundle pinning regime (left hatched region). The line $b_t(\delta)$ shows the amorphization transition line in the dense regime as described by Eq. (59) for bundle pinning and Eq. (61) for single-vortex pinning. For very weak pinning $\delta/\varepsilon < c_L^3$ as in NbSe this line is in the bulk pinning regime, for stronger disorder as in YBCO and BSCCO it lies in the single-vortex regime.

using Eqs. (10) and (39). This equation produces two branches for the single-vortex pinning field b_{sv}. For $b \ll 1$, where the factor $(1-b)$ can be neglected in Eq. (45), we find for the lower branch $b_{sv}^l \propto (\delta/\varepsilon)^{2/3}$ and close to the upper critical field $1-b \ll 1$, where the factor b can be neglected in Eq. (45), an upper branch $1 - b_{sv}^u \propto (\delta/\varepsilon)^{2/3}$, see Fig. 4. For $\delta/\varepsilon < \kappa^{-3}$ the lower branch enters the dilute regime $a > \lambda_{ab}$ where $b_{sv}^l \propto \kappa^{-2} \ln^{-2}(\kappa^{-1}\delta^{1/3})$; this is the generic situation for NbSe. For $\delta/\varepsilon > (8\pi)^{-3/2} \approx 0.008$ there is only single-vortex pinning; typical disorder strengths for YBCO and BSCCO have similar values.

Values for the pinning parameter δ/ε are higher in the high-T_c materials YBCO and BSCCO and the amorphization transition line at $T=0$ will lie in the single-vortex pinning regime whereas they are much lower in the rather isotropic low-T_c materials such as NbSe where the amorphization transition line typically starts out in the bundle pinning regime at $T=0$, see Fig. 4. For low-T_c materials the lower branch of the single-vortex pinning boundary b_{sv}^l is usually in the dilute regime $a > \lambda_{ab}$ due to the small disorder strength whereas in the high-T_c materials it is in the dense regime $a < \lambda_{ab}$. This is the experimental situation that we will assume throughout the following discussion of the different materials and that is sketched in Fig. 4.

The temperature dependence of the lines b_{sv} is rather different depending on whether the depinning temperature T_{dp} is much smaller then the critical temperature T_c as in the high-T_c materials YBCO and BSCCO or whether it practically coincides with T_c as in the low-T_c superconductor NbSe, see Fig. 5. Therefore the thermal weakening of disorder above the depinning temperature, which gives an exponential increase of the pinning length, is the dominant effect for high-T_c superconductors. The temperature dependence

FIG. 5. Schematic pinning diagram in the b-t plane showing the temperature dependence of the single-vortex pinning field b_{sv} for δl pinning (solid lines) and δT_c pinning (dashed lines). For the high-T_c materials YBCO and BSCCO thermal smoothing above the depinning temperature T_{dp} governs the temperature dependence of b_{sv}. For the low-T_c material NbSe the temperature dependence of the pinning parameter $\delta(t)$ itself [Eqs. (37) and (38)] is most relevant.

through the microscopic parameters (37) or (38) can be neglected for these materials as long as T_{dp}/T_c is small. In this situation we have to use the condition $L_0 = L_c(T)$ with $L_c(T)$ from Eq. (43) above the depinning temperature T_{dp}. This gives in the dense regime

$$b_{sv}(1-b_{sv}) \simeq 2\pi \left(\frac{\delta}{\varepsilon}\right)^{2/3} \left(\frac{T_{dp}}{T}\right)^2 e^{-2C(T/T_{dp})^\alpha} \qquad (46)$$

from which we derive an exponentially decreasing lower branch $b_{sv}^l(T) = b_{sv}^l(0)(T_{dp}/T)^2 \exp[-2C(T/T_{dp})^\alpha]$ [by neglecting factors of $(1-b)$ in Eq. (46)] and an exponentially increasing upper branch $1-b_{sv}^u(T) = [1-b_{sv}^u(0)]$ $\times (T_{dp}/T)^2 \exp[-2C(T/T_{dp})^\alpha]$ [by neglecting factors of b in Eq. (46)] as shown in Fig. 5. At temperatures slightly above T_{dp} the lower branch enters the dilute regime $a > \lambda_{ab}$. Note that for high-T_c materials $b_{sv}^l(T)$ typically starts out in the dense regime for $T=0$. The thermal weakening of disorder above T_{dp} has been neglected in Ref. 32 although high-T_c materials with potentially rather low T_{dp} have been considered.

On the other hand, T_{dp}/T_c is no longer small for the low-T_c superconductors where $T_{dp}/T_c \approx 1$, and in these materials the temperature dependence of the pinning length comes exclusively through the temperature dependence of the pinning strength (37) or (38). Using this in Eq. (45) we find $b_{sv}^l(t) \propto (1-t)$ and $1-b_{sv}^l(t) \propto (1-t)$ for δl pinning and $b_{sv}^l(t) \propto (1-t)^{-1/3}$ and $1-b_{sv}^l(t) \propto (1-t)^{-1/3}$ for δT_c pinning in the dense regime. If $b_{sv}^l(T)$ starts out in the dilute regime for $T=0$ the lower branch for δl pinning is $b_{sv}^l(T) \propto \kappa^{-2} \ln^{-2}[\kappa^{-1}\delta^{-1/3}(1-t)^{-1/2}]$ and stays in the dilute regime, see Fig. 5. For δT_c pinning the lower branch will enter into the dense regime at a temperature $1-t \simeq (\delta/\varepsilon)^2 \kappa^6$ in this case, see Fig. 5. Note that these results are very different from what has been obtained in Ref. 31 where factors $(1-b)$ in the expression for L_0 have been neglected.

C. Pinning of pancake vortices

On the smallest scale in a layered superconductor $L = d$ we can no longer discuss fluctuations of vortex *lines*. Then we have to consider the relative displacements $\mathbf{u} \equiv \Delta \mathbf{u}(d)$ between single pancake segments of the vortex line in two neighboring layers and discuss the pinning of single pancake vortices.[28,41,51,52] For large disorder strength and weak Josephson coupling as it occurs typically in BSCCO, it is possible that $\delta_d > 1$, which is equivalent to $L_c < d$ as becomes clear from the definition (36) of δ_d. In this case the pinning

of pancake vortices becomes particularly interesting because we cross over to a regime where pinning is no longer a small perturbation but we have *strong pinning* of pointlike pancake vortices. To calculate $\langle \Delta u^2(d) \rangle_T$ on the scale of the layer distance, we consider as in Sec. V B a single pancake with displacement $\mathbf{u}$ coupled to the pancakes in adjacent layers by a harmonic potential $\varepsilon_l (1/d) u^2/d$, but with an additional pinning potential $V_d(\mathbf{u}) = dV(0,\mathbf{u})$.

Using an Imry-Ma argument[28,41,51,52] one can estimate $\overline{\langle u \rangle^2}$ for strong pinning ($\delta_d > 1$) at low temperatures as follows. A vortex with displacement u can explore $\mathcal{N} = u^2/\xi_{ab}^2$ pinning sites with statistically independent disorder configurations. Doing so it can gain a pinning energy $E_{pin}(u) \simeq -U_p \ln^{1/2}(u^2/\xi^2)$ that can be determined from the condition $\mathcal{N} \int_{-\infty}^{E_{pin}(u)} dE\, p(E) \sim 1$. In the Imry-Ma argument the total energy $E(u) = E_{pin}(u) + (1/d)\varepsilon_l(1/d)u^2$ is minimized. The optimal disorder-induced displacement fluctuation u in the ground state is

$$u^2 \simeq \frac{dU_p}{\varepsilon_l(1/d)} \ln^{-1/2}\left(\frac{u^2}{\xi^2}\right). \qquad (47)$$

Solving the last equation iteratively yields

$$\overline{\langle u \rangle^2} \simeq \xi_{ab}^2 \delta_d^{1/2} \ln^{-1/2}(\delta_d^{1/2}). \qquad (48)$$

The corresponding ground-state energy $E_0 \simeq E_{pin}(u)$ is

$$E_0 \simeq -U_p \ln^{1/2}(\delta_d^{1/2}) \qquad (49)$$

whereas the typical elastic energy sets an energy scale $U^* \simeq (1/d)\varepsilon_l(1/d)u^2$,

$$U^* \simeq U_p \ln^{-1/2}(\delta_d^{1/2}), \qquad (50)$$

which is the typical size of elastic energy barriers between different metastable states.

Equation (48) is a nonperturbative result which holds for $\overline{\langle u \rangle^2} > \xi_{ab}^2$, which is exactly the condition $\delta_d > 1$ for strong pinning. Otherwise perturbation theory applies and one finds

$$\overline{\langle u \rangle^2}_{RF} \simeq \xi_{ab}^2 \delta_d, \qquad (51)$$

which is the perturbative RF result for weakly pinned pancake vortices.

Thermal fluctuations weaken the pinning and lead to thermal depinning of pinned pancakes. The characteristic depinning temperatures, however, are different for the cases of strong pinning ($\delta_d > 1$) and weak pinning ($\delta_d < 1$). For strong pinning the relevant depinning temperature is set by

the typical barrier height U^*, and the depinning happens in the temperature interval $U^* < T < |E_0|$.[41,52] For weak pinning the *pancake depinning temperature* $T_{dp,d}$ is determined in the usual way by the condition $\langle u^2 \rangle_T \simeq \xi_{ab}^2$ which gives

$$T_{dp,d} \simeq \varepsilon_l (1/d) \xi_{ab}^2 / d = U_p \delta_d^{-1/2}. \tag{52}$$

For weak pinning the resulting thermally weakened displacements are[41]

$$\overline{\langle u \rangle^2}_{RF} \approx \xi_{ab}^2 \delta_d \left(1 + \frac{T}{T_{dp,d}} \right)^{-2}. \tag{53}$$

For strong pinning the result (48) is valid up to a temperature $T \simeq U^*$ at which the thermal energy becomes sufficient to overcome barriers between minima of the pinning energy landscape. Therefore U^* is the depinning temperature for strongly pinned pancake vortices. For $U^* < T < |E_0|$ there is a crossover region where a modified random force result applies that decreases exponentially with increasing temperature before it crosses over to the thermally weakened random force result (53):[41]

$$\overline{\langle u \rangle^2}_{RF} \simeq \begin{cases} \xi_{ab}^2 \delta_d \left(1 + \dfrac{T}{U^*} \right)^{-2} \exp\left(-2 \dfrac{T}{U^*} \right) \\ \qquad \text{for } U^* < T < |E_0| \\ \xi_{ab}^2 \delta_d \left(\dfrac{T_{dp,d}}{T} \right)^2 \qquad \text{for } T > |E_0|. \end{cases} \tag{54}$$

What remains to be considered for strong pinning are the displacements on scales larger than d, i.e., the case $L > d > L_c$. At low temperatures, we are in the RM regime at all scales $L > d$ such that

$$\overline{\langle \Delta u \rangle^2}(L) \simeq \overline{\langle \Delta u \rangle^2}(d) \left(\frac{L}{d} \right)^{2\zeta_{RM}}, \tag{55}$$

where $\overline{\langle \Delta u^2 \rangle}(d)$ is given by Eq. (48), and $\zeta_{RM} \approx 5/8$. This result stays valid up to temperatures U^* where the strongly pinned pancakes thermally depin. At this temperature the thermally increased pinning length grows beyond the layer spacing $L_c(U^*) = d$, increases (double) exponentially for $U^* < T < |E_0|$, and crosses over to the weak pinning result (43) for $T > |E_0|$. The details of the (double-) exponential increase of $L_c(T)$ in the temperature interval $U^* < T < |E_0|$ for strong pinning are given in Ref. 41. The displacements $\overline{\langle \Delta u \rangle^2}(L)$ for $U^* < T < |E_0|$ are as in Eq. (44) given by

$$\overline{\langle \Delta u \rangle^2}(L) \simeq \langle \Delta u^2 \rangle_T [L_c(T)] \left(\frac{L}{L_c(T)} \right)^{5/4} \tag{56}$$

but with the altered strong pinning behavior of the pinning length $L_c(T)$. For $T > |E_0|$ Eq. (44) applies again.

VII. ORDER-DISORDER TRANSITION AT $T = 0$

In the presence of quenched point disorder the Lindemann criterion (4) for the stability of the BrG and thus the location of the order-disorder transition can be written as

$$\overline{\langle \Delta u(L_0) \rangle^2} = c_L^2 a^2, \tag{57}$$

where we used Eq. (9). As for thermal fluctuations we only need to consider displacement fluctuations of single vortices on scales $L < L_0$ using the results for pinned single vortices introduced in the preceding section. In this section we want to consider the case $T = 0$ and study the order-disorder or amorphization transition line $b_t(\delta)$ as function of the pinning strength only. The resulting phase diagrams in the b-δ plane are shown in Fig. 6 for NbSe, YBCO, and BSCCO.

A. NbSe, YBCO

At $T = 0$ the anisotropic type-II superconductors YBCO and NbSe have essentially identical phase diagrams in the b-δ plane if pinning is weak enough that a vortex is collectively pinned over distances $L_c > d$ and the layered structure of YBCO can be neglected.

For weak pinning in the dense regime $a < \lambda_{ab}$ we use the weak collective pinning theory and the anisotropic stiffness from the Josephson coupling, i.e., Eq. (40) for bundle pinning or Eq. (41) for single-vortex pinning to evaluate the left-hand side (lhs) $\overline{\langle \Delta u(L_0) \rangle^2}$ of the above Lindemann criterion. For very weak pinning the transition line will be in the bundle pinning regime where we use $L_0 \simeq \varepsilon a (1-b)^{-1/2}$ from Eqs. (10) and (40) to obtain

$$\overline{\langle \Delta u(L_0) \rangle^2} \simeq \xi_{ab}^2 \left(\frac{L_0}{L_c} \right)^3 \simeq a^2 \left(\frac{b}{2\pi} \right)^{-1/2} (1-b)^{-3/2} \frac{\delta}{\varepsilon}. \tag{58}$$

This result is interesting because it means that the Lindemann criterion (57) gives a order-disorder transition line $b_t(\delta)$ leading to a *reentrance* of the amorphous VG within the dense regime $a < \lambda_{ab}$ as long as we have bundle pinning. We find upper and lower branches of the reentrant transition line $b_t(\delta)$,

$$1 - b_t^u \simeq (2\pi)^{1/3} c_L^{-4/3} \left(\frac{\delta}{\varepsilon} \right)^{2/3},$$

$$b_t^l \simeq 2\pi c_L^{-4} \left(\frac{\delta}{\varepsilon} \right)^2, \tag{59}$$

which meet at $b_t = 1/4$ such that there is no transition line in the bundle pinning regime for disorders $\delta/\varepsilon > 0.13 c_L^2$, see Fig. 6. Using the condition $L_0 = L_c$ for b_{sv}, one finds that the order-disorder transition line $b_t(\delta)$ intersects the single-vortex pinning line $b_{sv}(\delta)$ for $c_L^2 a^2 = \overline{\langle \Delta u(L_c) \rangle^2} = \xi_{ab}^2$ and thus leaves the bundle pinning regime at a field $b_t = 2\pi c_L^2$ and a disorder strength $\delta/\varepsilon \approx c_L^3$, see also Fig. 4. Therefore, the peculiar reentrant behavior can only be found for $b_t = 2\pi c_L^2 < 1/4$ or Lindemann numbers $c_L < (8\pi)^{-1/2} \approx 0.2$. Note that our results for weak pinning in the dense regime are very different from the results of Ref. 31 as we treated high-field correction factors $(1-b)$ correctly. As indicated in Fig. 6, NbSe typically has a very small pinning parameter such that the upper order-disorder transition field is given by
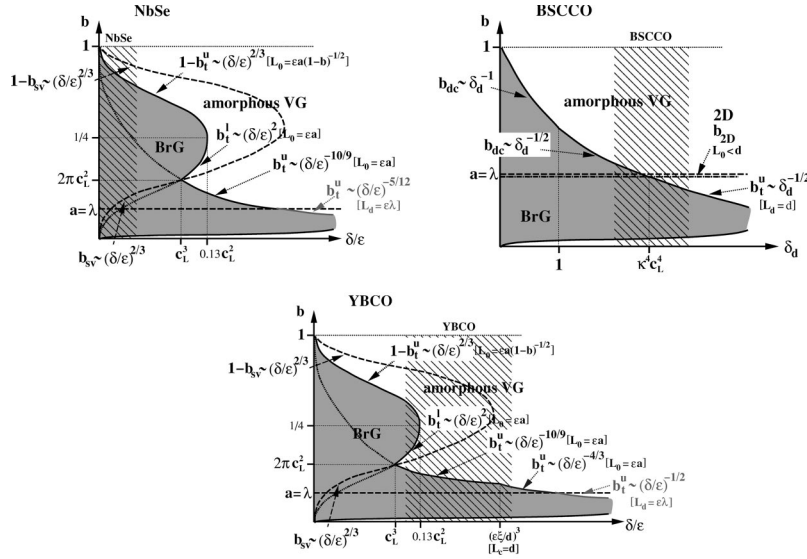
FIG. 6. Schematic phase diagram for NbSe and YBCO in the b-δ/ε plane, and for BSCCO in the b-δ_d plane (the dilute regime is enlarged, the reentrance of the amorphous VG at very low fields is shown for completeness but not discussed in the text). The diagram also contains the single-vortex pinning field b_{sv} marking the boundary between single-vortex pinning and bundle pinning, cf. Fig. 4. The hatched regions indicate a range of realistic disorder strengths for each material, cf. Fig. 4. The BrG is stable in the dark shaded regions. For NbSe and YBCO the order-disorder transition line b_t is given by Eq. (59) for bundle pinning and Eq. (61) for single-vortex pinning. Note that in the bundle pinning regime there can be an upper and lower branch leading to a reentrant amorphous VG phase. For YBCO with strong disorder we have $L_c < d$, and the upper branch of the order-disorder transition line in the single-vortex regime is given by Eq. (66) and (68). For BSCCO the order-disorder transition is given by Eqs. (69) and (70). The decoupling transition line b_{dc}, which is the continuation of the order-disorder transition line above the 2D crossover field b_{2D}.

the bundle pinning result (59). The lower transition field is then located within the dilute regime $a > \lambda_{ab}$, and not given by Eq. (59).

For stronger disorder $\delta/\varepsilon > c_L^3$, as it is typical for YBCO, there will be another transition line in the dense regime, which lies in the single-vortex pinning regime at magnetic fields $b_t < 2\pi c_L^2$, see Fig. 6. This part is found from Eqs. (41) and (10),

$$\overline{\langle \Delta u(L_0) \rangle^2} \simeq \xi_{ab}^2 \left(\frac{L_0}{L_c} \right)^{5/4} \simeq a^2 \left(\frac{b}{2\pi} \right)^{3/8} (1-b)^{-5/8} \left(\frac{\delta}{\varepsilon} \right)^{5/12}. \tag{60}$$

For single-vortex pinning, the Lindemann criterion (57) only gives an upper branch of the order-disorder transition line $b_t(\delta)$ at

$$b_t^u \simeq 2\pi c_L^{16/3} \left(\frac{\delta}{\varepsilon} \right)^{-10/9}, \tag{61}$$

where we used $1 - b \ll 1$ because $b_t^l < 2\pi c_L^2 \ll 1$ in the single-vortex regime. We conclude that there will be a reentrance of the amorphous VG and the BrG as function of the magnetic field for disorder strengths $c_L^3 < \delta/\varepsilon < 0.13 c_L^2$, see Fig. 6, if the Lindemann number c_L is sufficiently small. Only the result (61) for the order-disorder transition line in the single-vortex pinning regime, which can be more generally written as

$$b_t^u \sim c_L^{2/(1-\zeta_{RM})} \left(\frac{\delta}{\varepsilon} \right)^{-2\zeta_{RM}/3(1-\zeta_{RM})}, \tag{62}$$

has been obtained in all previous Lindemann analysis[25–32] which differ only in the estimates used for ζ_{RM}.

On the continuation of the upper branch of the order-disorder transition line into the dilute limit $a > \lambda_{ab}$ fluctuations on the scale $L_d = \varepsilon\lambda_{ab}$ govern the displacement fluctuations in the Lindemann criterion (57), i.e., $\overline{\langle \Delta u(L_0) \rangle^2} \simeq \overline{\langle \Delta u(\varepsilon\lambda_{ab}) \rangle^2}$. Only for single-vortex pinning disorder is strong enough ($\delta/\varepsilon > c_L^{24/5} \kappa^{9/5}$) that the upper branch of the amorphization line lies in the dilute regime. Thus we use Eqs. (41) and (10) to obtain

$$\overline{\langle \Delta u(\varepsilon\lambda_{ab}) \rangle^2} \simeq \xi_{ab}^2 \left(\frac{\varepsilon\lambda_{ab}}{L_c} \right)^{5/4} \simeq a^2 \frac{b}{2\pi} \kappa^{-5/4} \left(\frac{\delta}{\varepsilon} \right)^{5/12}, \tag{63}$$

which gives with the Lindemann criterion the upper branch of the order-disorder transition in the dilute regime,

$$b_t^u \simeq 2\pi c_L^2 \kappa^{-5/4} \left(\frac{\delta}{\varepsilon} \right)^{-5/12}. \tag{64}$$

B. YBCO

The YBCO phase diagram in the b-δ plane is qualitatively different from the NbSe diagram only for such strong disorder that the collective pinning length drops below the layer spacing $L_c < d$, see Fig. 6. This happens for $\delta/\varepsilon > (\varepsilon\xi/d)^3 = (\varepsilon/\varepsilon_d\kappa)^3$ [or $\delta_d = (\delta/\varepsilon)(\kappa\varepsilon_d/\varepsilon)^3 > 1$, see Eqs. (34) and (36)] in the single-vortex pinning regime; for generic disorder strengths in YBCO this also happens before the order-disorder transition line enters the dilute regime as

indicated in Fig. 6. For $L_c < d$ we have to use our results about strongly pinned pancake vortices from Sec. VI C). In particular, we have to use Eq. (55) together with Eq. (48) to calculate the lhs $\overline{\langle \Delta u(L_0) \rangle^2}$ in the Lindemann criterion (57).

In the dense limit $a < \lambda_{ab}$ the Josephson coupling and thus fluctuations on the scale L_0 dominate the displacements. Neglecting logarithmic corrections we find from Eqs. (55) and (48),

$$\overline{\langle \Delta u(L_0) \rangle^2} \simeq \xi_{ab}^2 \delta_d^{1/2} \left(\frac{L_0}{d} \right)^{5/4} \simeq a^2 \left(\frac{b}{2\pi} \right)^{3/8} \left(\frac{\varepsilon_d}{\varepsilon} \kappa \right)^{1/4} \left(\frac{\delta}{\varepsilon} \right)^{1/2},$$
(65)

which gives for the upper branch of the order-disorder transition in the dense limit[30]

$$b_t^u \simeq 2\pi c_L^{16/3} \left(\frac{\varepsilon_d}{\varepsilon} \kappa \right)^{-2/3} \left(\frac{\delta}{\varepsilon} \right)^{-4/3}.$$
(66)

Upon increasing the disorder strength, the order-disorder transition line enters the dilute limit [for $\delta/\varepsilon > c_L^4 (\varepsilon/\varepsilon_d \kappa)^{1/2} \kappa^{3/2}$], see Fig. 6. In the dilute limit, fluctuations on the scale $L_d = \varepsilon \lambda_{ab}$ cause the strongest displacements, for which Eqs. (55) and (48) yield

$$\overline{\langle \Delta u(\varepsilon \lambda_{ab}) \rangle^2} \simeq \xi_{ab}^2 \delta_d^{1/2} \left(\frac{\varepsilon \lambda_{ab}}{d} \right)^{5/4}$$

$$\simeq a^2 \frac{b}{2\pi} \left(\frac{\varepsilon_d}{\varepsilon} \kappa \right)^{1/4} \kappa^{5/4} \left(\frac{\delta}{\varepsilon} \right)^{1/2}$$
(67)

and hence for the upper branch of the order-disorder transition line in the dilute limit

$$b_t^u \simeq 2\pi c_L^2 \left(\frac{\varepsilon_d}{\varepsilon} \kappa \right)^{-1/4} \kappa^{-5/4} \left(\frac{\delta}{\varepsilon} \right)^{-1/2}.$$
(68)

This case has been previously studied in Ref. 28, the results of which agree with Eq. (68).

C. BSCCO

The strongly layered BSCCO has a weak Josephson coupling at low temperatures, and the 2D crossover field b_{2D} is slightly below the boundary to the dense regime according to Eq. (21). Consequently, the upper branch of the 3D amorphization transition line lies entirely in the dilute regime where fluctuations on the scale $L_d = d$ dominate on the lhs of the Lindemann criterion (57), $\overline{\langle \Delta u(L_0) \rangle^2} \simeq \overline{\langle \Delta u(d) \rangle^2}$.

In a strongly layered material such as BSCCO it is more convenient to use the parameter δ_d, see Eq. (36) for the disorder strength and discuss the order-disorder transition line in the b-δ_d plane. For weak pinning ($\delta_d < 1$) we use Eq. (51) to calculate for the upper branch of the order-disorder transition line in the dilute limit

$$b_t^u \simeq 2\pi c_L^2 \delta_d^{-1}.$$
(69)

On the other hand, for strong pinning ($\delta_d > 1$) we use Eq. (48) to obtain

$$b_t^u \simeq 2\pi c_L^2 \delta_d^{-1/2},$$
(70)

which agrees with the corresponding result of Ref. 28. For typical values $\kappa \approx 200$ for BSCCO it is clear that the order-disorder transition line intersects the 2D crossover field $b_{2D} \simeq 2\pi \kappa^{-2}$ in the strong pinning regime for $\delta_d \simeq c_L^4 \kappa^4$ (which usually entails $\delta_d \gg 1$). Note that typical pinning strengths for BSCCO have similar values, as indicated in Fig. 6. At smaller disorder strengths the BrG phase will be stable up to a decoupling field $b_{dc}(\delta_d)$ where the FLL decouples into 2D pancake lattices. As already mentioned there is no stable 2D BrG phase and we thus conclude that at the decoupling field also the in-plane topological order is lost and we have a direct transition into a 2D amorphous VG. If the decoupling transition is also described by a Lindemann criterion of the form

$$\overline{\langle \Delta u(0,d) \rangle^2} = c_L^2 a^2$$
(71)

as proposed in Ref. 51 the same formulas (69) and (70) apply to the decoupling transition line $b_{dc}(\delta_d)$, which is the continuation of the order-disorder transition line into the regime above the 2D crossover field b_{2D}, see Fig. 6. It should be stressed that the phase diagram of BSCCO in the b-δ plane looks qualitatively different from those of YBCO and NbSe in the dense regime $a < \lambda_{ab}$ at higher fields as the peculiar reentrance of the amorphous VG phase is absent for BSCCO because fluctuations on the scale of the layer spacing d are dominating for this material.

VIII. ORDER-DISORDER TRANSITION AT $T > 0$

In this section we discuss the influence of thermal fluctuations on the phase diagrams we derived in the preceding section for $T = 0$. To do so we choose a realistic $T = 0$ value for the disorder strength δ/ε or δ_d somewhere in the hatched regions of Fig. 6. The results for the phase diagrams of NbSe, YBCO, and BSCCO in the b-t plane are summarized in Fig. 7. Similar to what we found already for the single-vortex pinning field b_{sv} there are essential differences in the temperature dependence of the order-disorder transition line $b_t(t)$ depending on whether the depinning temperature T_{dp} is much smaller than the critical temperature T_c as in the high-T_c materials YBCO and BSCCO or whether it practically coincides with T_c as in the low-T_c superconductor NbSe. In the high-T_c materials the thermal weakening of the disorder which gives an exponential increase of the pinning length in Eq. (43) is by far the dominant effect. On the other hand, in the low-T_c materials T_{dp} is very close to T_c and the temperature dependence through the microscopic pinning parameters (37) or (38) is most important.

A. NbSe

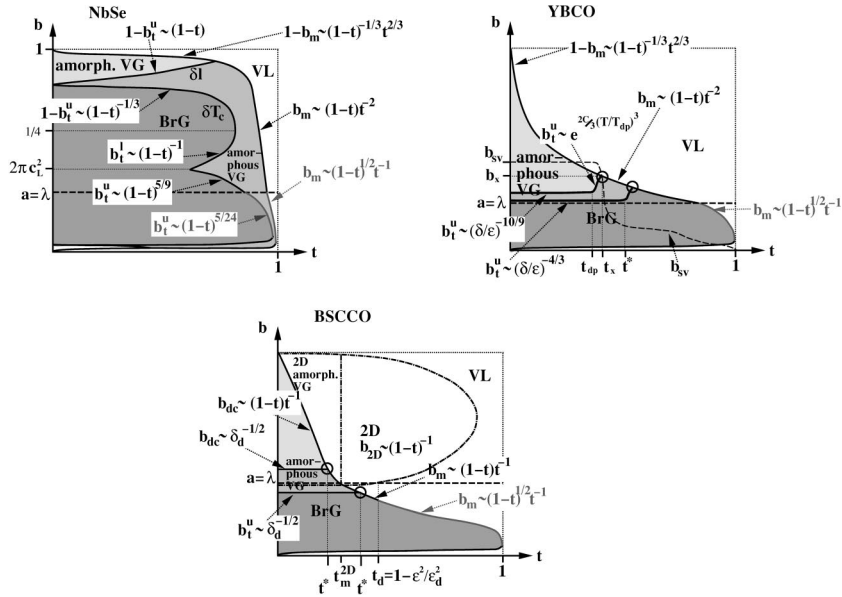In a low-T_c such as NbSe we typically have weak bundle pinning at the order-disorder transition at $T = 0$, and the

FIG. 7. Schematic phase diagram for NbSe, YBCO, and BSCCO in the b-t plane. (The dilute regime is enlarged, the reentrance at very low fields is shown for completeness but not discussed in the text.) The BrG is stable in the dark shaded regions. The amorphous VG phase occurs in the light shaded regions. The diagrams contain both the thermal melting lines b_m from Fig. 3 and the order-disorder transition lines b_t. For YBCO and BSCCO the order-disorder transition line is shown for two different disorder strengths; for the smaller disorder strength the stable BrG phase extends into the lighter shaded region. For NbSe the temperature dependence of the order-disorder transition line stems from the temperature dependence through microscopic parameters. The stable BrG phase for δT_c pinning is indicated by the dark shaded region, for δl pinning it extends also into the lighter shaded region to the right. For YBCO and BSCCO the temperature dependence mainly stems from thermal smoothing above the depinning temperature T_{dp}. For YBCO the order-disorder transition line is temperature independent below T_{dp} and given by Eq. (73) between T_{dp} and T_x, where it intersects the melting line and the single-vortex pinning line b_{sv}. For BSCCO the order-disorder transition line is generically temperature independent, i.e., horizontal and intersects the melting line at T_x $= U^*$ ($t^* \equiv U^*/T_c$).

order-disorder transition fields $b_t^{u,l}$ are given by Eq. (59) at $T=0$. Thermal depinning from disorder can be neglected, and the temperature dependence of the order-disorder transition line comes exclusively from the temperature dependence through the microscopic parameters entering the pinning strength δ, i.e., Eq. (37) or (38). Then, the order-disorder transition line in the b-t plane is obtained from Eqs. (59), (61), and (64) simply by substituting the correct $\delta(t)$ according to Eq. (37) or (38).

For δl pinning the disorder strength decreases with increasing temperature $\propto(1-t)^{3/2}$ which gives together with Eq. (59) an upper branch of the order-disorder transition line which stays in the bundle pinning regime and has a temperature dependence $1-b_t^u(t)\propto(1-t)$. Therefore, the order-disorder transition line approaches $b=1$ with increasing temperature and has to intersect the melting line $b_m(t)$ where it terminates, see Fig. 7. Because we used here the Lindemann criterion based on the scenario of two distinct instabilities for thermal and quenched fluctuations the phase diagram looks qualitatively as in Fig. 1 on the right. For a cooperative mechanism the transition line will be lower and *not* intersect the melting line as on the left in Fig. 1.

For δT_c pinning the situation is rather different because the disorder strength increases with temperature $\propto(1-t)^{-1/2}$ such that the BrG becomes always unstable sufficiently close to T_c and the order-disorder transition line does not intersect the melting line. Because the disorder strength

increases with temperature for δT_c pinning the topology of the phase diagram in the b-t plane is the same as that in the b-δ plane, as can be seen in Figs. 6 and 7. In particular the amorphous VG and the BrG are reentrant as a function of the magnetic field in the dense regime also in the b-t plane. Using Eq. (59) we find within the bundle pinning regime the two branches $1-b_t^u(t)\propto(1-t)^{-1/3}$ and $b_t^l(t)\propto(1-t)^{-1}$. In the single-vortex pinning regime (61) gives $b_t^u(t)\propto(1-t)^{5/9}$. Finally, the upper branch of the order-disorder transition line enters the dilute regime and with Eq. (64) we obtain $b_t^u(t)\propto(1-t)^{5/24}$. These results are summarized in Fig. 7.

Our results for the case of δT_c pinning might give an explanation for the experimental phase diagram measured in Ref. 23 where a reentrant amorphous VG phase was found in the dense regime which does not intersect with the melting line. This is exactly what we find for δT_c pinning in the bundle pinning regime, see Fig. 7. We also want to point out that our results are markedly different from what has been obtained in Ref. 31 where high-field correction factors ($1-b$) have been treated incorrectly.

B. YBCO

For the high-T_c materials YBCO and BSCCO the thermal smearing plays a much bigger role than the temperature de-

pendence through the microscopic parameters contained in the pinning strength δ. For YBCO effects from the layered structure can be neglected unless at rather high disorder strength $\delta/\varepsilon > (\varepsilon\xi/d)^3$ or $\delta_d > 1$ where $L_c(0) < d$. However, typical disorder strengths δ/ε for YBCO are bigger than for NbSe (due to the intrinsic doping of HTSC and the increased anisotropy) and the order-disorder transition field b_t^u is located within the single-vortex pinning regime at low temperatures.

For $L_c(0) > d$ collective pinning theory applies and the thermal smearing sets in above the depinning temperature T_{dp}. For $T < T_{dp}$ the order-disorder transition line $b_t^u(t)$ is horizontal and given by Eq. (61), see Fig. 7. In high-T_c materials T_{dp} is typically well below T_c. Taking typical values for YBCO as an anisotropic high-T_c superconductor with strong Josephson coupling, $\lambda_{ab} \approx 1500$ Å, $\varepsilon \approx 1/5$, $d \approx 12$ Å, and a disorder strength $\delta/\varepsilon \approx 10^{-2}$ [corresponding to a critical current $j_c \simeq j_0 (\delta/\varepsilon)^{2/3} \simeq 10^7$ A cm^{-2}], we have weak pinning [$L_c(0) > d$] and find $T_{dp} \simeq 40$ K for the depinning temperature, which is indeed well below $T_c \approx 90$ K. For $T > T_{dp}$ we have to use Eq. (44) to evaluate the lhs of the Lindemann criterion (57) and obtain

$$\overline{\langle \Delta u(L_0)\rangle^2} \simeq \xi_{ab}^2 \left(\frac{L_0}{L_c(0)}\right)^{5/4}\left(\frac{T}{T_{dp}}\right)^{5/4} e^{-(C/4)(T/T_{dp})^\alpha}$$

$$\simeq a^2 \left(\frac{b}{2\pi}\right)^{3/8}(1-b)^{-5/8}\left(\frac{\delta}{\varepsilon}\right)^{5/12}\left(\frac{T}{T_{dp}}\right)^{5/4}$$

$$\times e^{-(C/4)(T/T_{dp})^\alpha}. \tag{72}$$

Pinning-induced displacements drop exponentially above T_{dp}, therefore the thermal smearing is by far the most important effect of thermal fluctuations. The Lindemann criterion (57) yields an exponentially increasing upper branch of the order-disorder transition line

$$b_t^u \simeq 2\pi c_L^{16/3}\left(\frac{\delta}{\varepsilon}\right)^{-10/9}\left(\frac{T}{T_{dp}}\right)^{-10/3} e^{(2C/3)(T/T_{dp})^\alpha}, \tag{73}$$

which will intersect the melting line at a temperature T_x, which can be determined from a simple argument as follows. According to the scenario where thermal and quenched fluctuations cause independently instabilities of the BrG, thermal displacements should be of the *same* size as disorder-induced fluctuations at T_x, i.e., $\langle\Delta u^2(L_0)\rangle_T = \overline{\langle\Delta u(L_0)\rangle^2}$. However, this is exactly the definition of the pinning length $L_c(T)$ above the temperature T_{dp} from which we conclude that T_x is determined by the additional condition $L_c(T_x) = L_0$. This also means that the amorphization transition line $b_t^u(t)$ does not leave the single-vortex pinning regime for thermally weakened disorder above T_{dp} until it intersects also with the single-vortex pinning boundary $b_{sv}(t)$ (46) at T_x, see Fig. 7. For the temperature T_x and the field $b_x \equiv b_m(t_x) = b_t^u(t_x) = b_{sv}(t_x)$ we find

$$T_x \simeq T_{dp}\left(\frac{2}{C}\ln\left[(\delta/\varepsilon)^{1/3}c_L^{-1}\right]\right)^{1/\alpha}, \tag{74}$$

$$b_x \simeq 2\pi c_L^4\left(\frac{\delta}{\varepsilon}\right)^{-2/3}\left(\frac{T_x}{T_{dp}}\right)^{-2}. \tag{75}$$

The temperature T_x is only slightly above T_{dp} due to the exponential increase of the upper branch of the order-disorder transition line. Using a disorder strength $\delta/\varepsilon \approx 10^{-2}$ and $c_L \approx 0.15$ we obtain $B_x \approx 5.6$ T for the intersection field in good agreement with experimental phase diagrams for YBCO.[22] The characteristic exponentially increasing upper branch of the order-disorder transition line (73) above the depinning temperature T_{dp} has also been obtained in Refs. 25, 27, and 30.

For $L_c(0) < d$ pancake vortices are strongly pinned at low temperatures and the thermal smearing of the pinning potential sets in at the higher temperature U^* (50) which is the characteristic depinning temperature for strong pinning. For $T < U^*$ the order-disorder transition line $b_t^u(t)$ is horizontal and given by Eq. (66), see Fig. 7. At the temperature U^* we find $L_c(U^*) = d$, and in the temperature interval $U^* < T < |E_0|$ pinning-induced displacements decrease (double) exponentially with increasing temperature according to Eq. (56). For $T > |E_0|$ the results cross over to the above formula (73). The details of the (double) exponential increase of the order-disorder transition line $b_t^u(t)$ for $U^* < T < |E_0|$ can be easily obtained using the results of Ref. 41 but will not be presented here. The resulting phase diagram looks qualitatively as for weak pinning with the slightly higher $t^* = U^*/T_c$ replacing the depinning temperature t_{dp}, see Fig. 7.

Regardless of whether we have strong disorder with $L_c(0) < d$ or weak collective pinning, we find a remarkable reentrant nonmonotonic BrG instability line if we follow the order-disorder transition line $b_t^u(t)$ and after the intersection further on the thermal melting line $b_m(t)$, see Fig. 7. This is in agreement with experiments[22] where a nonmonotonic BrG instability line is clearly seen for YBCO. Because we used here the Lindemann criterion based on the scenario of two distinct instabilities for thermal and quenched fluctuations the phase diagram of YBCO in Fig. 7 looks qualitatively as in Fig. 1 on the right. For a cooperative mechanism the transition line $b_t^u(t)$ will be lower and *not* intersect the melting line as on the left in Fig. 1. However, also in this scenario a reentrant nonmonotonic behavior of the resulting curve $b_t^u(t)$ is found.

C. BSCCO

For the strongly layered BSCCO several phase diagrams in the b-t plane are possible depending on the three temperatures T_d, below which BSCCO has a weak Josephson coupling, the 2D melting temperature T_m^{2D}, and finally the characteristic depinning temperature U^*. For pancake pinning

energies U_p between $U_p \approx 10$ K and $U_p \approx 20$ K one finds values between $U^* \approx 5$ K and $U^* \approx 10$ K for the depinning temperature U^*.

As for the thermal melting we will focus on the situation $T_m^{2D} < T_d$ that occurs for a realistic choice of material parameters for BSCCO; in Sec. V B we found estimates $T_d \approx 36$ K and $T_m^{2D} \approx 10$ K. Then the upper branch of the 3D melting line lies entirely in the dilute regime as in Fig. 3. Typical disorder strengths for BSCCO are such that we are in the strong pinning regime $\delta_d > 1$. For sufficiently strong disorder $\delta_d > c_L^4 \kappa^4 (\gg 1)$, which corresponds to $U^* > T_m^{2D}$, there is a genuine 3D amorphization transition at $T = 0$ whereas for smaller disorder $1 < \delta_d < c_L^4 \kappa^4$, corresponding to $U^* < T_m^{2D}$, we have found a decoupling transition that simultaneously destroys topological in-plane order.

For strong disorder $\delta_d > c_L^4 \kappa^4$ or $U^* > T_m^{2D}$ the 3D amorphization transition field b_t^u lies in the dilute regime at low temperatures and its disorder dependence is given by Eq. (70). Thermal fluctuations lead to a depinning of strongly pinned pancake vortices only above the temperature U^* at which $\overline{\langle \Delta u(d) \rangle^2} \simeq \langle \Delta u(d)^2 \rangle_T$.[41] Therefore U^* is also the temperature where the amorphization transition line $b_t^u(t)$ intersects the melting line, i.e., $T_x = U^*$. For all $T < U^*$ the amorphization transition line runs horizontally, see Fig. 7. In particular, this excludes a reentrant behavior. The horizontal order-disorder transition line $b_t^u(t)$ and, after intersecting, the thermal melting line $b_m(t)$ are monotonously decreasing with increasing temperature. This is unchanged also if we use the slightly different Lindemann criterion based on a cooperative mechanism of thermal and quenched fluctuations. Indeed, experimental signs for a nonmonotonic BrG instability line are much weaker for the BSCCO compound,[21] and only recently a small "inverse melting" effect has been confirmed experimentally.[53] Because the nonmonotony is much smaller in BSCCO than in YBCO this effect might be beyond the scope of the Lindemann criterion for BSCCO. Above the order-disorder transition line $b_t^u(t)$ we can speculate that a 3D amorphous VG phase will be stable up to the thermal decoupling field $b_{dc}(t)$ that we discussed in Sec. V B. At $b_{dc}(t)$ the FLL decouples by thermal fluctuations into 2D pancake lattices which are in a 2D amorphous VG phase as there is no stable 2D BrG phase. The 2D amorphous VG phase might be separated by another dynamical crossover, in which the dislocation mobility increases by thermal fluctuations, from the 2D VL phase but both phases have no in-plane topological order.

For somewhat weaker disorder $1 < \delta_d < c_L^4 \kappa^4$ or $U^* < T_m^{2D}$ a slightly different sequence of transitions occurs as at low temperatures the BrG phase is stable up to a decoupling field b_{dc}, which lies in the dense regime and the disorder dependence of which is also given by the right-hand side of Eq. (70). As there is no stable 2D BrG phase the FLL decouples directly into the 2D amorphous VG at b_{dc}. If the locus of this line is as well determined by a Lindemann criterion such as Eq. (71), we obtain as for the amorphization transition line a temperature-independent, horizontal transition line $b_{dc}(t)$ that intersects the thermal melting line at a

temperature $T_x = U^*$, see Fig. 7. However, there will be no subsequent thermal decoupling in this case but eventually another temperature-driven crossover to the 2D VL phase.

IX. CONCLUSION

In conclusion, we have presented a comparative and comprehensive Lindemann analysis of the melting line and the stability boundaries of the Bragg glass phase, i.e., the amorphization transition line for the three superconducting materials of most intense experimental interest: the high-T_c materials YBCO and BSCCO and the low-T_c superconductor NbSe. We find that it is important to distinguish between slightly different versions of the Lindemann criterion depending on whether quenched disorder-induced and thermal fluctuations act cooperatively or independently in destroying the lattice order. The two versions can actually be linked to different scenarios for the proliferation of topological defects in the destruction of the Bragg glass phase.

Special attention is paid to the role of the electromagnetic coupling for the strongly layered compound BSCCO and to the different mechanism of temperature dependence in the pinning strength. We find that in high-T_c materials thermal smearing of the pinning potential is most important whereas in the low-T_c material NbSe the temperature dependence through the microscopics of the pinning mechanism determines the phase behavior. Taking also into account high-field corrections to the elastic moduli we obtain results regarding the phase diagram of the low-T_c material NbSe which are markedly different from earlier findings[31] and which give a reentrant amorphous VG phase in the dense regime very similar to what has been observed in recent experiments.[23]

APPENDIX: MATERIAL PARAMETERS AND LIST OF SYMBOLS

For the low-T_c compound NbSe we use the following set of material parameters:

$$T_c \approx 6 \text{ K},$$

$$\varepsilon \approx 1/3,$$

$$\xi_{ab} \approx 100 \text{ Å},$$

$$\lambda_{ab} \approx 2000 \text{ Å}, \tag{A1}$$

TABLE I. List of symbols. Our notation is mostly adapted from Ref. 1.

a	FLL spacing	
b_{dc}	Decoupling transition field	
b_m	Thermal melting field	
b_{sv}	Single-vortex pinning field	Eqs. (45) and (46)
b_t	Order-disorder or amorphization transition field	
b_x	Intersection field of b_m and b_t	
b_{2D}	2D crossover field	Eq. (21)
γ	Pinning strength parameter	Eq. (33)
c_L	Lindemann number	Eq. (1)
$c_{44}(K,q)$, c_{66}	(Dispersive) FLL tilt modulus, FLL shear modulus	Eq. (11)
d	Layer spacing	
E_0	Pancake ground-state energy	Eq. (49)
δ	Pinning strength parameter	Eqs. (34), (37), and (38)
δ_d	Layered pinning strength parameter	Eq. (36)
$\varepsilon = \lambda_{ab}/\lambda_c$	Anisotropy ratio	
ε_d	Layered anisotropy	Eq. (18)
$\varepsilon_l(q)$	(Dispersive) single-vortex line tension	Eq. (12)
$\varepsilon_0 = (\Phi_0/4\pi\lambda_{ab})^2$	Characteristic line energy	
Gi	Ginsburg number	Eq. (23)
Gi_{2D}	2D Ginsburg number	
j_c	Single-vortex critical current	
j_0	Depairing current	
λ_{em}	Scale for onset of electromagnetic dispersion	Eqs. (13) and (15)
$\tilde{\lambda}_{ab}$	Effective magnetic penetration depth	Eq. (14)
L_c	Collective pinning or Larkin length	Eqs. (39) and (43)
L_d	Dispersion length scale	Eq. (17)
L_0	Single-vortex length	Eq. (6)
T_d	Crossover temperature to strong Josephson coupling	Eq. (19)
T_{dp}	Depinning temperature	Eq. (42)
$T_{dp,d}$	Pancake depinning temperature	Eq. (52)
T_m	Thermal melting temperature	
T_m^{2D}	2D melting temperature	
T_x	Intersection temperature of b_m and b_t	
U_p	Pancake pinning energy	Eq. (35)
U^*	Pancake energy barrier	Eq. (50)

which leads to $\kappa \approx 20$, $\mathrm{Gi} \approx 1.7 \times 10^{-6}$. NbSe has no layered structure which can be formally considered as the limit $\varepsilon_d \approx 0$. Pinning is typically weak with $\delta/\varepsilon \approx 10^{-9}$.

For the moderately anisotropic high-T_c compound YBCO we use

$$T_c \approx 90 \text{ K},$$

$$\varepsilon \approx 1/5,$$

$$\xi_{ab} \approx 15 \text{ Å},$$

$$\lambda_{ab} \approx 1500 \text{ Å},$$

$$d \approx 12 \text{ Å}, \tag{A2}$$

which leads to $\kappa \approx 100$, $\mathrm{Gi} \approx 10^{-2}$, and $\varepsilon_d \approx 0.008 \ll \varepsilon$. A typical pinning strength is $\delta/\varepsilon \approx 10^{-2}$.

For the strongly layered high-T_c material BSCCO we use

$$T_c \approx 100 \text{ K},$$

$$\varepsilon \approx 1/200,$$

$$\xi_{ab} \approx 100 \text{ Å},$$

$$\lambda_{ab} \approx 2000 \text{ Å},$$

$$d \approx 15 \text{ Å}, \tag{A3}$$

which leads to $\kappa \approx 200$, $\mathrm{Gi}_{2D} \approx 0.096$, $T_m^{2D} \approx 10$ K, $\varepsilon_d \approx 0.0075 > \varepsilon$, and $T_d \approx 36$ K. A typical value for the pinning parameter is $\delta_d \approx 10^4 \gg 1$ corresponding to $U_p \approx 10$ K.

[1] G. Blatter, M.V. Feigelman, V.B. Geshkenbein, A.I. Larkin, and V.M. Vinokur, Rev. Mod. Phys. **66**, 1125 (1994).

[2] E.H. Brandt, Rep. Prog. Phys. **58**, 1465 (1995).

[3] T. Nattermann and S. Scheidl, Adv. Phys. **49**, 607 (2000).

[4] D.R. Nelson, Phys. Rev. Lett. **60**, 1973 (1988).

[5] H. Safar, P.L. Gammel, D.A. Huse, D.J. Bishop, J.P. Rice, and D.M. Ginsberg, Phys. Rev. Lett. **69**, 824 (1992); R. Liang, D.A. Bonn, and W.N. Hardy, *ibid.* **76**, 835 (1996); U. Welp, J.A. Fendrich, W.K. Kwok, G.W. Crabtree, and B.W. Veal, *ibid.* **76**, 4809 (1996); E. Zeldov, D. Majer, M. Konczykowski, V.B. Geshkenbein, V.M. Vinokur, and H. Shtrikman, Nature (London) **375**, 373 (1995).

[6] D.R. Nelson and H.S. Seung, Phys. Rev. B **39**, 9153 (1989); A. Houghton, R.A. Pelcovits, and A. Sudbø, *ibid.* **40**, 6763 (1989).

[7] G. Blatter, V. Geshkenbein, A. Larkin, and H. Nordborg, Phys. Rev. B **54**, 72 (1996).

[8] M.J.W. Dodgson, A.E. Koshelev, V.B. Geshkenbein, and G. Blatter, Phys. Rev. Lett. **84**, 2698 (2000).

[9] J. Kierfeld and V. Vinokur, Phys. Rev. B **61**, R14 928 (2000).

[10] A.I. Larkin, Sov. Phys. JETP **31**, 784 (1970); A.I. Larkin and Y.N. Ovchinnikov, J. Low Temp. Phys. **34**, 409 (1979).

[11] M.P.A. Fisher, Phys. Rev. Lett. **62**, 1415 (1989).

[12] M.V. Feigelman, V.B. Geshkenbein, A.I. Larkin, and V.M. Vinokur, Phys. Rev. Lett. **63**, 2303 (1989).

[13] R.H. Koch, V. Foglietti, W.J. Gallagher, G. Koren, A. Gupta, and M.P.A. Fisher, Phys. Rev. Lett. **63**, 1511 (1989).

[14] D.S. Fisher, M.P.A. Fisher, and D.A. Huse, Phys. Rev. B **43**, 130 (1991).

[15] T. Nattermann, Phys. Rev. Lett. **64**, 2454 (1990).

[16] T. Giamarchi and P. Le Doussal, Phys. Rev. Lett. **72**, 1530 (1994); Phys. Rev. B **52**, 1242 (1995).

[17] J. Kierfeld, T. Nattermann, and T. Hwa, Phys. Rev. B **55**, 626 (1997).

[18] D.S. Fisher, Phys. Rev. Lett. **78**, 1964 (1997).

[19] R. Cubitt, E.M. Forgan, G. Yang, S.L. Lee, D.M. Paul, H.A. Mook, M. Yethiraj, P.H. Kes, T.W. Li, A.A. Menovsky, Z. Tarnawski, and K. Mortensen, Nature (London) **365**, 407 (1993).

[20] H. Safar, P.L. Gammel, D.A. Huse, D.J. Bishop, W.C. Lee, J. Giapintzakis, and D.M. Ginsberg, Phys. Rev. Lett. **70**, 3800 (1993).

[21] B. Khaykovich, E. Zeldov, D. Majer, T.W. Li, P.H. Kes, and M. Konczykowski, Phys. Rev. Lett. **76**, 2555 (1996).

[22] S. Kokkaliaris, P.A.J. de Groot, S.N. Gordeev, A.A. Zhukov, R. Gagnon, and L. Taillefer, Phys. Rev. Lett. **82**, 5116 (1999).

[23] Y. Paltiel, E. Zeldov, Y. Myasoedov, M.L. Rappaport, G. Jung, S. Bhattacharya, M.J. Higgins, Z.L. Xiao, E.Y. Andrei, P.L. Gammel, and D.J. Bishop, Phys. Rev. Lett. **85**, 3712 (2000).

[24] J. Kierfeld, H. Nordborg, and V.M. Vinokur, Phys. Rev. Lett. **85**, 4948 (2000).

[25] D. Ertaş and D.R. Nelson, Physica C **272**, 79 (1996).

[26] Y.Y. Goldschmidt, Phys. Rev. B **56**, 2800 (1997).

[27] T. Giamarchi and P. Le Doussal, Phys. Rev. B **55**, 6577 (1997).

[28] A.E. Koshelev and V.M. Vinokur, Phys. Rev. B **57**, 8026 (1998).

[29] V. Vinokur, B. Khaykovich, E. Zeldov, M. Konczykowski, R.A. Doyle, and P.H. Kes, Physica C **295**, 209 (1998).

[30] J. Kierfeld, Physica C **300**, 171 (1998).

[31] G.P. Mikitik and E.H. Brandt, Phys. Rev. B **64**, 184514 (2001).

[32] Y. Radzyner, A. Shaulov, Y. Yeshurun, I. Felner, K. Kishio, and J. Shimoyama, Phys. Rev. B **65**, 100503 (2002); Y. Radzyner, A. Shaulov, and Y. Yeshurun, *ibid.* **65**, 100513 (2002).

[33] S. Ryu, S. Doniach, G. Deutscher, and A. Kapitulnik, Phys. Rev. Lett. **68**, 710 (1992).

[34] H. Nordborg and G. Blatter, Phys. Rev. Lett. **79**, 1925 (1997).

[35] X. Hu, S. Miyashita, and M. Tachiki, Phys. Rev. B **58**, 3438 (1998).

[36] D.S. Fisher, M.P.A. Fisher, and D.A. Huse, Phys. Rev. B **43**, 130 (1991).

[37] T. Hwa and D.S. Fisher, Phys. Rev. B **49**, 3136 (1994).

[38] T. Nattermann, S. Scheidl, S.E. Korshunov, and M.S. Li, J. Phys. I **5**, 565 (1995).

[39] S. Scheidl, Phys. Rev. B **55**, 457 (1997).

[40] E.H. Brandt, J. Low Temp. Phys. **26**, 735 (1977).

[41] J. Kierfeld (unpublished).

[42] J.R. Clem, Phys. Rev. **43**, 7837 (1991).

[43] G. Blatter, M. Dodgson, and V. Geshkenbein, Physica C **332**, 66 (2000).

[44] C. Zeng, P.L. Leath, and D.S. Fisher, Phys. Rev. Lett. **82**, 1935 (1999); P. Le Doussal and T. Giamarchi, Physica C **331**, 233 (2000).

[45] M. Müller, D.A. Gorokhov, and G. Blatter, Phys. Rev. B **64**, 134523 (2001).

[46] D.A. Gorokhov and G. Blatter, Phys. Rev. B **62**, 14 032 (2000).

[47] S.S. Banerjee, N.G. Patil, S. Saha, S. Ramakrishnan, A.K. Grover, S. Bhattacharya, G. Ravikumar, P.K. Mishra, T.V. Chandrasekhar Rao, V.C. Sahni, M.J. Higgins, E. Yamamoto, Y. Haga, M. Hedo, Y. Inada, and Y. Onuki, Phys. Rev. B **58**, 995 (1998).

[48] L.I. Glazman and A.E. Koshelev, Phys. Rev. B **43**, 2835 (1991).

[49] J.M. Kim and J.M. Kosterlitz, Phys. Rev. Lett. **62**, 2289 (1989).

[50] T. Halpin-Healy and Y.C. Zhang, Phys. Rep. **254**, 215 (1995).

[51] A.E. Koshelev, L.I. Glazman, and A.I. Larkin, Phys. Rev. B **53**, 2786 (1996).

[52] O.S. Wagner, G. Burkard, V.B. Geshkenbein, and G. Blatter, Phys. Rev. Lett. **81**, 906 (1998).

[53] N. Avraham, B. Khaykovich, Y. Myasoedov, M. Rappaport, H. Shtrikman, D.E. Feldman, T. Tamegai, P.H. Kes, M. Li, M. Konczykowski, K. van der Beek, and E. Zeldov, Nature (London) **411**, 451 (2001).